Lyl-1 marks and regulates primitive macrophages and microglia development

Shoutang Wang[1, †, *], Deshan Ren[1, ††, *], Anna-Lila Kaushik[1, †††], Gabriel Matherat[1, ††††], Yann Lécluse[2], Dominik Filipp[3], William Vainchenker[1], Hana Raslova[1], Isabelle Plo[1], Isabelle Godin[1]

[1] Gustave Roussy, INSERM U1287, Villejuif; Université Paris-Saclay, France.

[2] PFIC, lUMS AMMICa (US 23 INSERM / UMS 3655 CNRS; Gustave Roussy, Villejuif, France

[3] Laboratory of Immunobiology, Institute of Molecular Genetics of the Czech Academy of Sciences, Prague, Czech Republic.

Present addresses: [†] Department of Pathology and Immunology, Washington University School of Medicine, St. Louis, MO, 63110, USA; [††] Medical school of Nanjing university, Model Animal Research Center, Nanjing University, Nanjing 210093, China; [†††] Plasseraud IP, 33064 Bordeaux, France; [††††] INSERM U1016, CNRS UMR8104, Institut Cochin, Université de Paris, Paris, France

***** Equal contribution;

Short Title: Lyl-1 in macrophage/microglia ontogeny

Corresponding author:

Isabelle Godin (ORCID: 0000-0001-8577-8388)

INSERM U1287; Institut Gustave Roussy-PR1; 114, rue Edouard Vaillant; 94805 VILLEJUIF Cedex; France

Email address: Isabelle.Godin@gustaveroussy.fr ;

Phone: (33) 142 11 41 43; Fax: (33) 142 11 52 40

Key points:

1- Lyl-1 expression marks yolk sac macrophages and brain macrophage/microglia/BAM.

2- Lyl-1 deficiency impairs primitive macrophage development and leads to the up-regulation of genes involved in embryo patterning.

3- Lyl-1-expressing primitive macrophages have an immuno-modulatory phenotype.

4- Lyl-1 deficiency impairs microglia development and the expression of genes involved in neuro-development.

Abstract

During ontogeny, resident macrophages (MΦs) of the nervous system emerge from haematopoietic stem cell-independent progenitors originating in the Yolk Sac (YS), so that factors impairing YS MΦ development may lead to neurodevelopmental disorders resulting from defective brain resident MΦ.

Here we show that Lyl-1, a bHLH transcription factor related to Scl/Tal-1, marks primitive macrophage ($M\Phi^{Prim}$) progenitors in the YS. Transcriptomic analysis of YS MΦ progenitors indicated that $M\Phi^{Prim}$ progenitors present at embryonic day (E) 9 are clearly distinct from those present at E10. Lyl-1 bHLH disruption led to an increased production and a defective differentiation of $M\Phi^{Prim}$ progenitors. These differentiation defects were associated with profound modifications of the expression of genes involved in embryonic patterning and neurodevelopment. They also induced a reduced production of mature MΦ/microglia in the early brain, as well as a transient reduction of the microglia pool at midgestation and in the new-born.

We thus identify Lyl-1 as a critical regulator of $M\Phi^{Prim}$ and microglia development, which disruption may impair organogenesis, including neurodevelopment processes.

INTRODUCTION

Amongst the components of the transcription factor network that regulate the various features of haematopoietic cells, Tal-1, Lmo2, Runx1 and Gata2 stand out as the major regulators of haematopoietic progenitor development during ontogeny *(Pina and Enver, 2007; Wilson et al., 2010)*. *Tal-1*, *Lmo2* and *Gata-2* belong to a transcriptional complex, which also includes the basic helix-loop-helix (bHLH) transcription factor lymphoblastic leukaemia-derived sequence 1 (*Lyl-1*). Contrary to its paralog *Tal-1*, which is mandatory for the specification of all haematopoietic progenitors *(Curtis et al., 2012; Porcher et al., 2017)*, the function of Lyl-1 during developmental haematopoiesis remains largely unknown. We therefore analysed this function using *Lyl-1*$^{LacZ/LacZ}$ mutant mice *(Capron et al., 2006)*, focusing on the initial steps of haematopoietic cells development in the yolk sac (YS).

During ontogeny, haematopoietic progenitors are generated in three successive waves *(Palis, 2016)*. The two first occur in the YS prior to Haematopoietic Stem Cell (HSC) generation. This HSC-independent haematopoiesis comprises first the primitive haematopoietic wave, with the transient production of monopotent progenitors with embryonic specific features. The second YS wave, called transient-definitive, provides for a limited duration progenitors (mostly erythro-myeloid) that seed the foetal liver (FL) and produce a haematopoietic progeny that displays definitive/adult differentiation features. Finally, HSC, generated in the aorta region in the third and definitive haematopoietic wave, immediately migrate to the FL where they mature and amplify to ultimately provide the population that will maintain lifelong haematopoiesis in the adult *(Cumano and Godin, 2007; Kieusseian et al., 2012)*.

During YS haematopoiesis, MΦ arising from the two waves derive either from a monopotent MΦ progenitor in the primitive wave *(Bertrand et al., 2005b; Palis et al., 1999)* or from the progressive differentiation of EMP via the production of GM progenitors, and ultimately of

granulocytes (G) and MΦ progenitors in the transient-definitive wave in a cMyb-dependent pathway *(McGrath et al., 2015)*.

In the recent years, fate-mapping approaches aimed at determining the embryonic origin of tissue resident MΦs indicated that most tissues harbour resident MΦs of various origins, such as YS, FL and adult bone marrow (reviewed in *(Ginhoux and Guilliams, 2016; Hoeffel and Ginhoux, 2018)*), which complicates the characterisation of the functions of the various MΦ subsets. In the case of brain resident MΦs, fate-mapping analyses established that, contrary to others tissue, these resident MΦs (microglia and Border Associated MΦ (BAM)) develop only from MΦ progenitors originating from the YS *(Ginhoux et al., 2010; Gomez Perdiguero et al., 2015; Kierdorf et al., 2013; Schulz et al., 2012; Utz et al., 2020)*, confirming a developmental model we had previously put forward *(Alliot et al., 1999)*. However, the wave (or waves) of origin remained unclear due to the limited criteria that discriminate progenitors from the two YS waves.

We here show that, at the early stages of YS haematopoiesis, *Lyl-1* expression discriminates primitive ($M\Phi^{Prim}$) from transient-definitive ($M\Phi^{T\text{-}Def}$) MΦ progenitors. In the brain, Lyl-1 marked the entire microglia/BAM population at the onset of brain colonisation and appeared to regulate microglia/BAM development.

Altogether, these data point to Lyl-1 as a major regulator of early embryonic MΦ progenitors development and advocate for further analyses to more precisely delineate Lyl-1 function during the development of resident MΦ in homeostatic and pathological contexts.

RESULTS

Lyl-1 expression discriminates MΦ^{Prim} from MΦ$^{T\text{-}Def}$ progenitors in the early YS

Since *Lyl-1* is expressed in the YS from the onset of haematopoiesis *(Giroux et al., 2007)*, we first explored its function by characterizing the progenitors produced by WT, *Lyl-1$^{WT/LacZ}$* and *Lyl-1$^{LacZ/LacZ}$* YS in clonogenic assay. To do so, YS at embryonic day (E) 8 were maintained in organ culture for 1 day (E8 OrgD1-YS), allowing only the development of progenitors from both primitive and transient-definitive waves *(Cumano et al., 1996; Cumano et al., 2001)*. Compared to WT, the production of MΦ colonies was increased in *Lyl-1$^{WT/LacZ}$* and *Lyl-1$^{LacZ/LacZ}$* OrgD1-YS. Otherwise, the clonogenic potential and colony distribution were unmodified ***(Fig. 1a)***.

Using FACS-Gal assay ***(Sup. fig 1a)***, we noticed that the entire MΦ progenitor population (cKit^{+}CD45^{+}CD11b^{+}) expressed Lyl-1 at E9. In contrast, from E9.5 (as in E8-OrgD1-YS), two MΦ progenitor subsets discriminated by FDG/Lyl-1 expression were present ***(Fig. 1b)***, suggesting that Lyl-1 may mark MΦ^{Prim} progenitors from the earliest wave. After E9.5, the YS harbours both MΦ^{Prim} and MΦ$^{T\text{-}Def}$ progenitors from the two YS waves and these two progenitors subsets cannot be discriminated by phenotype *(Bertrand et al., 2005b)*. We therefore investigated the known features that discriminate the two YS waves such as the origin from monopotent progenitors beginning at E7.25 for primitive progenitors *(Bertrand et al., 2005b; Palis et al., 1999)* or, for the transient-definitive progenitors, their progressive differentiation from EMP via the production of GM progenitors, and ultimately of granulocytes (G) and MΦ progenitors *(McGrath et al., 2015)* and the dependence on *cMyb* expression for their production *(Hoeffel et al., 2015; Schulz et al., 2012)*.

FACS-Gal assay performed at E8 (0-5S), when only MΦ^{Prim} are present, demonstrated that all early MΦ^{Prim} progenitors, characterised by a CD11b^{+}CD31^{+} phenotype *(Bertrand et al., 2005b)*, displayed FDG/Lyl-1 expression ***(Fig. 1c)***. Most FDG^{+}/Lyl-1^{+} cells (69.27%±0.33%) from *Lyl-1$^{WT/LacZ}$*

E8-YS co-expressed CD11b and CD31 and consistently produced MΦ colonies (72.78±9.65%; n=3) in clonogenic assays, amounting 1-4 MΦ progenitors per YS, a value consistent with previously published data *(Bertrand et al., 2005b; Palis et al., 1999)*.

As $M\Phi^{T\text{-}Def}$ arise from EMPs that also generate GM progenitors and granulocytes *(McGrath et al., 2015)*, we characterized the differentiation potential of FDG^{+}/Lyl-1^{+} and FDG^{-}/Lyl-1^{-} fractions of myeloid progenitors ($Ter119^{-}cKit^{+}CD45^{+}CD11b^{+}$) from E10 YS in clonogenic assay ***(Fig. 1d)***. All samples produced few non-myeloid contaminants, such as EMk and EMP in similar, non-significant amounts. Similar to WT E9-YS $M\Phi^{Prim}$ progenitors, E10 FDG^{+}/Lyl-1^{+} progenitor subset nearly exclusively produced MΦ colonies, confirming the restriction of Lyl-1 expression to $M\Phi^{Prim}$ progenitors. In contrast, E10 FDG^{-}/Lyl-1^{-} myeloid progenitors produced GM, G and MΦ colonies, confirming their multipotent/transient-definitive status.

The restriction of Lyl-1 expression to $M\Phi^{Prim}$ progenitors was also strengthened by RT-qPCR comparison of *cMyb* expression: FDG^{-}/Lyl-1^{-} progenitors displayed *cMyb* levels similar to Lineage negative $Sca1^{+}cKit^{+}$ progenitors from E12-FL, whereas, as E9-YS $M\Phi^{Prim}$ progenitors, FDG^{+}/Lyl-1^{+} YS progenitors expressed low *cMyb* levels, strengthening their primitive status ***(Fig. 1e)***.

A distinct separation of E9 and E10 MΦ progenitors was also confirmed in RNA-seq analysis of MΦ progenitors ($CD45^{+}CD11b^{+}cKit^{+}$) sorted at E9, when the YS contains only $M\Phi^{Prim}$ progenitors, and at E10, when it contains both $M\Phi^{Prim}$ and $M\Phi^{T\text{-}Def}$ progenitors. Principal Component Analysis pointed to a separation between E9 and E10 samples in both WT and *Lyl-1*$^{LacZ/LacZ}$ YS (PC1) and a separation between WT and *Lyl-1*$^{LacZ/LacZ}$ samples (PC2) clearer at E9 in frame with the restriction to $M\Phi^{Prim}$ progenitors at this stage ***(Fig. 1f)***.

E9 and E10 WT MΦ progenitors differed by the expression of 726 genes. Amongst the differentially expressed genes (DEGs), 176 were up-regulated at E9 and 550 at E10. Considering the presence of both $M\Phi^{Prim}$ and $M\Phi^{T\text{-}Def}$ progenitors in E10-YS, the DEGs found at this stage may

reflect either waves-specific differences or stage-dependent changes related to the maturation of MΦ^{Prim} progenitors.

Overlapping the identified DEGs to those obtained by Mass *et al*. *(Mass et al., 2016)* to characterise EMP and E10.25-E10.5 MΦs confirmed that E9 MΦ^{Prim} progenitors were clearly distinct from these two populations. While about 5% of E10 WT up-regulated genes belonged to the EMP and MΦ signatures, these genes represented respectively 27.5% and 35.6% of these signatures ***(Fig. 1g)***. A similar separation was also observed in Gene Set Enrichment Analysis (GSEA) ***(Sup. fig. 1b)***. These observations suggest that within E10 MΦ progenitors some, likely the MΦ$^{T\text{-}Def}$ ones, retain part of the EMPs signature.

Focusing on the differences with E10 MΦ progenitors in a WT context, E9 MΦ^{Prim} progenitors were found to differ from E10 progenitors by their transcription factors (TF) repertoire. E10 WT MΦ progenitors were enriched in genes associated with erythroid development (*Gata1, Gata2, Klf1*), as well as globin genes, both embryonic (*Hbb-bh1, Hba-x, Hbb-y*) and definitive (*Hba-a2, Hba-a1, Hbb-bt*) ***(Fig. 1g)***. E9 and E10 MΦ progenitors both exhibited a high expression of Spi1/PU.1 compared to Gata1 ***(Fig. 1h)***. The higher expression level of erythroid genes and of genes involved in granulo-monocytic (*Mpo, Csf2r/GM-CSF receptors, Cebp, Jun*) and megakaryocytic development (*Pf4, TPO signalling*) ***(Fig. 1g, Sup. table 1)*** at E10 sustains the notion that MΦ$^{T\text{-}Def}$ progenitors retain the expression of genes that characterize their EMP ancestor, as well as the monopotent status of E9 progenitors ***(Fig.1d)***.

Altogether, these data validate the monopotent/primitive status of E9 MΦ progenitors. However, due to the simultaneous presence of MΦ^{Prim} and MΦ$^{T\text{-}Def}$ progenitors in E10-YS, the differential expressions of makers that are wave-specific at this stage, such as *Lyl-1* for the primitive wave and *cMyb* and *Tlr2* *(Balounova et al., 2019)* for the transient-definitive one, were

not significant despite a net tendency to a decrease for *Lyl-1* and an increase for *cMyb* and *Tlr2* ***(Sup. fig. 1c)***.

Through QIAGEN's Ingenuity® Pathway (IPA) and GSEA analyses, it appeared that MΦ^{Prim} progenitors were more active in Eicosanoid signalling than E10 progenitors ***(Fig. 1i)***. E9 MΦ^{Prim} progenitors were also enriched in type I interferon (IFN) β and type II IFNγ signalling ***(Fig. 1j)*** and, as a consequence, in MHC-II related genes, especially *Cd74* (top 1 IPA network) ***(Fig. 1k; Sup. fig. 1d)***. Flow cytometry analyses confirmed a low, but significant, enrichment of MHC-II expression in E9 MΦ compared to E10 progenitors ***(Sup. fig. 1e)***. For their part, E10 MΦ progenitors were more active in inflammatory signalling ***(Fig. 1i, l; Sup. fig. 1d, f-h; Sup. table 1)***. They were also more metabolically active than E9 MΦ progenitors ***(Sup. table 1)***. In addition, the complement cascade and phagocytosis also prevailed at E10 ***(Sup. fig. 1i, j)***.

Lyl-1 deficiency in MΦ^{Prim} leads to patterning defects

During YS development, both MΦ^{Prim} and MΦ$^{T\text{-}Def}$ progenitors originate from cKit^{+}CD31^{+}CD45^{-} progenitors (C subset), which differentiate into MΦσ via 3 subsets (A1 to A3) *(Bertrand et al., 2005b)* ***(Sup. fig. 2a)***. When evaluating the effect of *Lyl-1* deficiency at the earliest stage of MΦ^{Prim} development, both FACS-Gal and clonogenic assays pointed to an increased production of MΦ progenitors in E8 *Lyl-1$^{WT/LacZ}$* compared to WT-YS ***(Fig. 2a)***, concordant with our first observation ***(Fig. 1a)***. The high increase of the expression level of *Itgα2b*/CD41 in *Lyl-1$^{lacZ/lacZ}$* MΦ^{Prim} progenitors ***(Fig. 2b)*** may reflect the elevated commitment of mesodermal/pre-haematopoietic cells to a MΦ fate ***(Sup. data and sup fig. 2b-d)***.

We noticed a clear-cut modification of the TF network ***(Fig. 2c)*** that controls developmental haematopoiesis *(Wilson et al., 2010)*: beside the expected reduction of *Lyl-1* expression, the expression of *Lmo2*, a target of *Lyl-1* *(McCormack et al., 2013)*, was also down-regulated, while

Tal-1 up-regulation might reflect a compensatory role *(Curtis et al., 2012)*. The consequence of these changes on early stages of YS development were apparent in GSEA analyses: both pathways and GO terms uncovered a general up-regulation of signalling pathways involved in early stages of embryo patterning (Wnt, Hox and Smad) in *Lyl-1*$^{LacZ/LacZ}$ MΦ progenitors, as well as deep changes in collagen, integrin and cadherin usage ***(Sup. table 2)***. Accordingly, various developmental trajectories were affected ***(Fig. 2d)***, with an up-regulation in E9 *Lyl-1*$^{LacZ/LacZ}$ MΦ progenitors of gene sets related to "anterior-posterior pattern specification" and "anatomical structure formation involved in morphogenesis", notably skeletal and nervous system development.

Another patterning modification was observed when comparing *Lyl-1*$^{LacZ/LacZ}$ to WT MΦ progenitors at E10: at this stage, GSEA and KEGG analyses pointed to the down-regulation of gene sets involved in heart development ***(Sup. fig. 2e; Sup. table 3)***. The heart harbours three resident MΦ subsets, two of which originate from the YS. Some of the features that differentiate the two CCR2^{-} YS-derived subsets *(Epelman et al., 2014)* also characterize E9 MΦ^{Prim} progenitors (high MHC-II expression ***(Fig. 1k)*** and low phagocytosis ability ***(Sup. fig. 1j)***. Therefore, a function for *Lyl-1* in heart development may be considered.

These patterning defects, which appear triggered by defective MΦ^{Prim} may be responsible, at least in part, for the significant decreased of litter size and increased perinatal lethality ***(Sup. fig. 2f)*** observed in *Lyl-1*$^{LacZ/LacZ}$ mice compared to WT, which indicates the requirement for functional Lyl-1 during various developmental processes.

Defective MΦ^{Prim} development in Lyl-1 mutants

We next monitored the distribution of A1-A2 and A3 MΦ subsets ***(Sup. fig. 2a)*** at E10-YS, when all three subsets are present, using the *Cx3cr1*$^{WT/GFP}$*:Lyl-1*$^{LacZ/LacZ}$ double knock-in strain. The

analysis of *Lyl-1* expression in A1-A2-A3 subsets from *Cx3cr1*$^{WT/GFP}$ YS at E10 indicated that *Lyl-1* is expressed throughout MΦ differentiation, with a level decreasing from A1 to A3 ***(Sup. fig. 3a)***.

The subset distribution was highly impacted by *Lyl-1* deficiency, leading to an increased A1 and a reduced A2 and A3 pool sizes ***(Fig. 3a)***. Thus, Lyl-1 appears to regulate MΦ progenitors differentiation towards mature MΦ. This defective differentiation could originate from the altered cytokine signalling uncovered in E9 mutant progenitors through GSEA and IPA analyses ***(Fig. 3b; Sup. fig. 3b)***. A limited or delayed differentiation of E9 MΦ^{Prim} progenitors was supported by the decreased expression of *Ptprc*/CD45, *Csfr1, Itgam*/CD11b and CD33 ***(Fig. 3c)***. The PU.1 signalling pathway was also decreased in E9 *Lyl-1*$^{LacZ/LacZ}$ progenitors ***(Sup. fig. 3c; Sup. table 4b)***.

Lyl-1$^{LacZ/LacZ}$ MΦ progenitors were also deficient in the IFN signalling that characterize E9 MΦ^{Prim} progenitors, notably *Irf8*, a factor involved in the development of YS-MΦ and microglia *(Hagemeyer et al., 2016; Kierdorf et al., 2013)* ***(Fig. 3d)***. Compared to WT progenitors, progenitors from *Lyl-1*$^{lacZ/lacZ}$ E9-YS up-regulated the LXR/RXR activation pathway ***(Fig. 3e)***, as well as various metabolic pathways, including some enriched in E10 WT progenitors (Butanoate and steroid) ***(Sup. table 1)***, and other which were not (Fructose/mannose and Fatty acid) ***(Fig. 2d)***. They were also less active in inflammatory signalling pathways, particularly through NFkB, a factor known to interact with *Lyl-1* *(Ferrier et al., 1999)*, and in TLR signalling (*Tlr4*, *Tlr7*, *Tlr8*, *Tlr9*) ***(Fig. 3d; Sup. fig. 3b, d-e; Sup. table 4b)***.

To better identify the core signature of *Lyl-1* deregulation taking into account the maturation that occur between E9 and E10, we overlapped DEGs identified in *Lyl-1*$^{LacZ/LacZ}$ MΦ progenitors at both stages. From the 16 DEGs common to both stages ***(Fig. 3f)***, only one, *Fcgr2b*, showed an opposite deregulation during development, being first down-regulated in the mutant at E9, then expressed at higher levels than in the WT at E10.

Lyl-1$^+$ MΦ progenitors contribute to the early brain and foetal liver.

The foetal liver *(Kieusseian et al., 2012)* and brain *(Alliot et al., 1999; Ginhoux et al., 2010)* are both colonised as early as E9 by YS-derived resident MΦ progenitors. We therefore implemented a FACS-Gal assay to evaluate the contribution of Lyl-1-expressing MΦ^{Prim} progenitors to these rudiments at E10 ***(Fig. 4a)***. While E10-YS comprised both FDG$^+$/Lyl-1$^+$ and FDG$^-$/Lyl-1$^-$ MΦ progenitor and mature (F4/80$^+$) MΦ subsets ***(Fig. 1b)***, the brain from the same embryos essentially harboured FDG$^+$/Lyl-1$^+$ MΦ progenitors and mature MΦ. In contrast, MΦ progenitors of both phenotypes (FDG$^+$/Lyl-1$^+$ and FDG$^-$/Lyl-1$^-$) were present in the FL, as in E10-YS. MΦ progenitors were more abundant in mutant FL than in WT ***(Fig. 4b)***, as in the YS, but the amount of mature MΦ was unmodified (Data not shown).

We next focused on brain MΦ during the colonisation stage, which occurs until E11 *(Matcovitch-Natan et al., 2016)*. At this stage, microglia and perivascular, meningeal and choroid plexus MΦ, collectively refered to as BAMs, are all located in the brain mesenchyme and are therefore undistinguishable *(Goldmann et al., 2016; Utz et al., 2020)*. FACS-Gal assay demonstrated that the whole F4/80$^+$ microglia/BAM population expresses Lyl-1 throughout the settlement period ***(Fig. 4c)***. The presence of Lyl-1$^+$ F4/80$^+$ microglia/BAM at the earliest stage of brain colonisation suggests that already differentiated MΦ could participate to the colonization step.

A lineage relationship between Lyl-1$^+$ MΦ^{Prim} progenitors and early microglia/BAM is therefore strongly considered, based on the timing of their appearance and on similar features, such as the low level of *cMyb* expression ***(Fig. 4d)***, concordant with the cMyb-independent development of microglia *(Kierdorf et al., 2013; Schulz et al., 2012)*. Such a putative lineage relationship is also supported by our RNA-seq data. WT E9 MΦ^{Prim} progenitors expressed

significantly lower levels of *Mrc1*/CD206 than E10 MΦ progenitors, as well as a significantly higher level of *Sall3* and a slight increase of *Sall1* ***(Fig. 4e)***, a transcriptomic pattern that characterises microglia *(Lavin et al., 2014; Mass et al., 2016; Matcovitch-Natan et al., 2016)*. This pattern suggests that E9-YS $M\Phi^{Prim}$ progenitors show a partial bias toward a microglia signature. These observations point to E9 $M\Phi^{Prim}$ progenitors as a likely source of embryonic microglia with the first stage of microglia development program already initiated in YS $M\Phi^{Prim}$ progenitors at E9.

We next examined the distribution of A1-A2 and A3 MΦ subsets in the brain of E10 $Cx3cr1^{WT/GFP}$:$Lyl\text{-}1^{LacZ/LacZ}$ embryos to assess the impact of *Lyl-1* deficiency at the onset of brain colonisation. *Lyl-1* expression levels in the brain MΦ subsets were similar to those observed in the YS ***(Fig. 4f, Sup. fig. 3a)***. However, *Lyl-1* deficiency led to an increased A1 and a reduced A3 pool size ***(Fig. 4g)***, indicating that in the brain, as in the YS, Lyl-1 regulates the differentiation of MΦ progenitors towards mature microglia/BAM.

Lyl-1 inactivation impairs microglia development at two development stages

Having defined Lyl-1 implication during microglia/BAM settlement in the brain, we turned to later development stages, focusing on $CD45^{lo}$ microglia. Cytometry and database analyses *(Matcovitch-Natan et al., 2016)* confirmed the continuous expression of Lyl-1 in microglia until adulthood ***(Sup. fig. 4a)***. We therefore examined the impact of *Lyl-1* inactivation on microglia pool size during development. Microglia quantification pointed to E12 as the first step impacted by the mutation**.** The arrested increase of the microglia pool in $Lyl\text{-}1^{LacZ/LacZ}$ brain at E12 ***(Fig. 5a)*** resulted from a reduced proliferation ***(Fig. 5b)*** rather than an increased apoptosis ***(Sup. fig. 4b)***. Moreover, *Lyl-1* deficiency also provoked morphological changes in E12 $Cx3cr1^{WT/GFP}$:$Lyl\text{-}1^{LacZ/LacZ}$ microglia, which displayed a reduced number and extent of ramifications compared to $Cx3cr1^{WT/GFP}$ microglia ***(Fig. 5c; Sup. fig. 4c, d)***. Interestingly, from E14, the microglia pool size

returned to levels similar to WT embryos *(Fig. 5a)*, a recovery that may result from the sharp reduction of apoptosis in *Lyl-1*$^{LacZ/LacZ}$ microglia at E14 *(Sup. fig. 4b)*.

P0-P3 was identified as a second development stage altered in *Lyl-1*$^{LacZ/LacZ}$ microglia. At birth, the cellularity of *Lyl-1*$^{LacZ/LacZ}$ brain was significantly decreased compared to WT *(Fig. 5d)*, which was not the case at earlier stages *(Sup. fig. 4e)*. The recovery of CD11b^{+} cells was also reduced (WT: 140.96±0.91x10^{3}; n=9; *Lyl-1*$^{LacZ/LacZ}$: 87.18±0.37x10^{3}; n=9). Consequently, *Lyl-1* deficiency triggered a nearly 2-fold reduction of the microglia population *(Fig. 5d)*. This perinatal reduction of the microglia pool appeared transient, since no difference with WT brain was observed in the adult *(Sup. fig. 4f)*. At perinatal stages, the reduction of brain cellularity in *Lyl-1*$^{LacZ/LacZ}$ mice points to Lyl-1 as a possible regulator of the trophic function of microglia on brain cells *(Antony et al., 2011; Ueno et al., 2013)*.

The identification of E12 and P0-P3 as key stages for Lyl-1 function in microglia development was confirmed by RT-qPCR analyses of the expression of genes essential for MΦ (*Spi1/*PU.1, *Csf1r*, *Mafb*) and/or microglia (*Runx1*, *Cx3cr1*, *Irf8*) development and function, as well as known regulators of developmental haematopoiesis (*Tal-1, Lmo2, Runx1*) and related factors (*Tcf3*/E2A, *Tcf4*/E2.2) *(Fig. 5e, f; Sup. fig. 4g)*. Time course analyses highlighted the down-regulation of *Csf1r*, *Irf8* and *Lmo2* in *Lyl-1*$^{LacZ/LacZ}$ microglia at both E12 and P0-P3, while *Cx3cr1* was only decreased at E12 *(Fig. 5g)*. Note that *Lyl-1* expression was unmodified in *Cx3cr1*$^{GFP/GFP}$ mutants *(Fig. 5g)*. Interestingly, *Cx3cr1*, as well as *Irf8* and *Lmo2*, belong to potential Lyl-1 target genes *(Wilson et al., 2010)*.

Mafb expression levels in *Lyl-1*$^{LacZ/LacZ}$ microglia transiently decreased at P0-P3 and later returned back to WT expression levels *(Fig. 5h)*. As Mafb represses resident MΦ self-renewal *(Soucie et al., 2016)*, this transient decrease may be linked to the recovery of a normal amount of microglia after perinatal stages. *Spi1/*PU.1, *Tcf3*/E2A and *Tcf4*/E2.2 expression levels were

unmodified in *Lyl-1*$^{LacZ/LacZ}$ microglia at any stage, while *Runx1* expression was only affected after birth. The expression of *Tal-1* was decreased at E14 and increased after birth, suggesting that this *Lyl-1* paralog *(Curtis et al., 2012)* does not compensate for *Lyl-1* deficiency during embryonic stages of microglia development, but may do so during postnatal stages ***(Sup. fig. 4g)***.

Remarkably, our RNA-seq results indicate that the expression level of some of the genes deregulated in *Lyl-1*$^{LacZ/LacZ}$ microglia at E12 and in the new-born were also down-regulated in *Lyl-1*$^{LacZ/LacZ}$ MΦ progenitors at E9 (*Csfr1:* ***Sup. fig. 3c***, *Lmo2:* ***Fig. 2c***; *Irf8:* ***Fig. 3d***; *Cx3cr1:* ***Fig. 5i)***. The de-regulation of these genes in microglia was transient, however in both locations and stages they coincided with a defective *Lyl-1*$^{LacZ/LacZ}$ MΦ/microglia differentiation.

Other genes enriched in microglia (*Fcrls*, *Mef2c*, *Maf*) *(Crotti and Ransohoff, 2016)* or involved in the maintenance of microglia homeostasis (*P2ry12*) *(Bisht et al., 2018)* were also expressed in E9 *Lyl-1*$^{LacZ/LacZ}$ MΦ progenitors at a lower level than in the WT**,** with exception of *Lpr8* and *Aif-1/*Iba1 which expression levels were increased ***(Fig. 5i)***. The deregulation of these genes might underlie the relationship between MΦ^{Prim} progenitors and microglia/neural development which became apparent upon *Lyl-1* inactivation considering the large number of neural signalling pathways up-regulated in E9 *Lyl-1*$^{LacZ/LacZ}$ MΦ progenitors ***(Fig. 2d)*** and the relationship of the DEGs enriched in E9 MΦ^{Prim} progenitors with brain formation and neuro-development uncovered in IPA analysis ***(Sup. fig. 4h)***.

Altogether, these data suggest that Lyl-1 deficiency in microglia may lead to neuro-developmental defects.

DISCUSSION

We here identified Lyl-1 as a marker for YS-derived MΦ^{Prim} progenitors and found that, at the earliest stage of YS development, this expression discriminated MΦ^{Prim} progenitors from those produced in the transient-definitive waves. The early expression of Lyl-1 in YS mesoderm *(Giroux et al., 2007)*, where it cannot substitute for the mandatory function of its paralog Tal-1 for the generation of haematopoietic progenitors *(Porcher et al., 2017)*, has already been established (reviewed in *(Curtis et al., 2012)*). More recently, Lyl-1 was also identified as a regulator of mesoderm cell fate in human induced pluripotent stem cells (iPSC) *(Palpant et al., 2017)*, and its function in the maintenance of primitive erythroid progenitors has been described *(Chiu et al., 2019)*. Parallel to Lyl-1 expression in the earliest wave of MΦ progenitor generation, our RNA-seq data now reveal Lyl-1 as an essential regulator in the specification of YS mesoderm to a haematopoietic fate since its invalidation affects major sets of genes involved in embryo patterning. Whether Lyl-1 role during the onset of organogenesis is specific to mesodermal stage or related to a patterning function for MΦ^{Prim} progenitors remains to be determined. Lyl-1 involvement in two discrete developmental steps of embryogenesis would constitute yet another similarity with its paralog Tal-1, which regulates both YS mesoderm determination to a haematopoietic fate and the differentiation of primitive erythroid cells *(Curtis et al., 2012)*.

Within the MΦ lineage, Lyl-1 function during normal development would initially consist to restrict the size of the MΦ^{Prim} progenitor pool and/or the duration of its production, which is thought to be transient *(McGrath et al., 2015)*, as shown by the increased size of this pool observed in *Lyl-1*$^{LacZ/LacZ}$ E8-E9 YS. Lyl-1 would also promote MΦ differentiation, when this process starts at E9.5, as the maintenance of an increased size of MΦ^{Prim} progenitor pool in *Lyl-1*$^{LacZ/LacZ}$ E10-YS appears to result from a defective cytokine signalling.

We also defined a signature for WT MΦ^{Prim} progenitors at E9, which comprises the Eicosanoid, MHC-II and IFN signalling pathways, pointing to an immuno-modulatory function for these MΦ^{Prim} progenitors. Comparatively, MΦ progenitors at E10 were rather involved in the response to bacteria and viruses, through phagocytosis and inflammatory signalling, with the preferential expression of TNF, TLR and TGFβ signalling pathways. Unfortunately, the simultaneous presence of MΦ^{Prim} and MΦ$^{T\text{-}Def}$ progenitors at E10 makes it difficult to attribute the changes of gene expression to a stage dependent maturation of MΦ^{Prim} progenitors or to a signature specific to MΦ$^{T\text{-}Def}$ progenitors. However it indicates that most pathways favoured by MΦ progenitors at E10 were insensitive to *Lyl-1* invalidation, except TLR signalling pathway that was down-regulated in E9 mutant MΦ progenitors, compared to WT.

The limitations of the current Lyl-1 model call for the development of new mouse models that will allow lineage specific reports of Lyl-1 expression and function in endothelial or haematopoietic lineages during discrete steps of early YS development and beyond. These extended investigations would probably improve our knowledge of other HSC-independent lineages, and benefit to the Embryonic Stem Cells/iPSC field in which the production of definitive cells types is complicated by the poor discrimination between primitive and definitive populations.

When analysing the contribution of Lyl-1^{+} MΦ progenitors to resident MΦ, we detected their presence in FL and brain rudiments right from the onset of their colonisation. In the developing brain, microglia/BAM maintained Lyl-1 expression and shared with MΦ^{Prim} progenitors a low level of *cMyb* expression. While fate-mapping analyses were instrumental to firmly ascribe a YS origin to microglia *(Ginhoux et al., 2010) (Kierdorf et al., 2013; Schulz et al., 2012) (Gomez Perdiguero et al., 2015)*, this strategy could not ascertain which YS progenitor wave contributes to microglia *(Mass, 2018; McGrath et al., 2015; Wittamer and Bertrand, 2020)*. Indeed, an

independent/specific targeting of only one MΦ progenitors wave was prevented by: 1- the similar phenotype of $M\Phi^{Prim}$ and $M\Phi^{T\text{-}Def}$ progenitors *(Bertrand et al., 2005b)*; 2- the short time-span separating the two YS waves (E7.25 and E8.25); 3- the high variability of development stages of individual embryos within a litter at these stage *(Downs and Davies, 1993)* and 4- the duration of TAM induction, now admitted to last up to 72h *(Senserrich et al., 2018)*. Using an *ex vivo* approaches whereby expression and potential can be examined in individually staged embryos, we found that, at least between E8 and E10, Lyl-1 expression discriminates $M\Phi^{Prim}$ from EMP-derived $M\Phi^{T\text{-}Def}$ progenitors, and also marks the entire embryonic microglia/BAM populations.

We therefore favour a model ascribing microglia origin to Lyl-1 $M\Phi^{Prim}$ progenitors, as they preferentially expressed genes belonging to the microglia signature (*Sall1 and Sall3, P2ry12, Mef2c, Fcrls*), while E10 MΦ progenitors favoured the expression of genes (*Id3*, *Runx3*), belonging to resident MΦ signatures in the lung and skin *(Mass et al., 2016)*. Even though a later contribution of $M\Phi^{T\text{-}Def}$ progenitors could be considered, provided they up-regulate Lyl-1 expression at a later stage, such model is supported by the low level of *cMyb* expressed by both Lyl-1^{+} $M\Phi^{Prim}$ progenitors and Lyl-1^{+} microglia, in frame with the intact microglia pool in *cMyb*-deficient mice *(Kierdorf et al., 2013; Schulz et al., 2012)* arguing for an origin of microglia from $M\Phi^{Prim}$ rather than $M\Phi^{T\text{-}Def}$ progenitors. Another argument comes from the zebrafish model where the fate of $M\Phi^{Prim}$ progenitors is more easily traced than in mammals as they arise from a location distinct from other haematopoietic progenitors *(Ferrero et al., 2018; Herbomel et al., 2001)*. Finally, this model is supported by the recent report that in mice lacking the ligand for cKit, the impaired development of EMPs leads to the depletion of resident MΦs in the skin, lung and liver, but does not affect the development of microglia *(Azzoni et al., 2018)*.

Some confusion in the identification of the YS progenitors that gives rise to microglia stems from the fact that both YS waves produce cells from erythro-myeloid lineages, hence the "early EMP" and "late EMP" terminology used to qualify the brain-seeding MΦ progenitor. The monopotent/ primitive nature of E9 MΦ progenitors was confirmed by our RNA-seq data, so that the $M\Phi^{Prim}$ progenitors terminology seems more appropriate than "early EMP" to qualify the primitive progenitors that give rise to microglia/BAM *(Ginhoux et al., 2010; Utz et al., 2020)*, particularly because $M\Phi^{Prim}$ and $M\Phi^{T\text{-}Def}$ progenitors clearly constitute distinct entities that need to be better discriminated in order to investigate their respective contribution and function in the tissues resident MΦ contributed by the YS.

Amongst the features that distinguish WT E9 $M\Phi^{Prim}$ progenitors from those present at E10, the enriched expression of MHC-II and the poor expression at E9 of genes related to phagocytosis also characterise one of the two YS-derived $CCR2^{-}$ resident MΦ subsets identified in the heart *(Epelman et al., 2014; Leid et al., 2016)*. A function for Lyl-1-expressing resident MΦ in cardiac development thus appears probable considering also the down-regulation of gene sets related to heart development and function in E10 *Lyl-1*$^{LacZ/LacZ}$ MΦ progenitors. This observation reinforces the need to better characterise the respective contributions of both YS-waves to resident MΦ in the tissues known to harbours YS-derived resident MΦ.

By investigating Lyl-1 function at later stages of microglia development, we identified E12 and P0-P3 as key stages impacted by *Lyl-1* deficiency. These time points correspond respectively to the end of "early-" (E9-E12) and "pre"-microglia" (E14-P9) stages of the microglia development program *(Matcovitch-Natan et al., 2016)*. Based on the gene expression pattern of *Lyl-1*-deficient microglia and the signature of $M\Phi^{Prim}$ progenitors in the early YS, a major contribution of *Lyl-1*-deficiency to neurodevelopmental disorders may be considered. Synaptic pruning and neural maturation, which characterise the perinatal phase of microglia development *(Matcovitch-Natan*

et al., 2016), might be impaired in *Lyl-1*$^{LacZ/LacZ}$ embryos considering the defects observed at P0-P3, the later key developmental stage regulated by Lyl-1.

Considering the sustained expression of Lyl-1 in microglia during adulthood, and the down-regulation of genes essential for microglia function in *Lyl-1*$^{LacZ/LacZ}$ microglia at E12 and P0-P3, Lyl-1 deregulation might contribute to various neuro-degenerative/neuro-inflammatory diseases and possibly play a role in the development of brain tumours. Such an involvement of Lyl-1 in the development of neuropathies is suggested by its deregulation in various pathological models of brain myeloid cells, uncovered through the analyses of brain myeloid cells datasets *(Friedman et al., 2018)* (http://research-pub.gene.com/BrainMyeloidLandscape/#Mouse-gene/Mouse-gene/17095/geneReport.html). Moreover, *LYL-1* expression was also reported in human microglia from healthy adult frontal cortex *(Wehrspaun et al., 2015)* and some reports highlight the relevance of LYL-1 deregulation in human neuro-developmental and neuro-degenerative diseases *(Colangelo et al., 2002; Thomas et al., 2006)*. Finally, *LYL-1* belongs to the 5 genes commonly deleted in patients suffering from 19p13.13 micro-deletions, which might contribute to the neuro-developmental disabilities *(Nimmakayalu et al., 2013)*. However, since Lyl-1 is expressed in endothelial cells, including in the brain *(Pirot et al., 2010)*, a possible contribution of *LYL-1*-deficient endothelial cells to these diseases should be considered.

Altogether, our findings reveal Lyl-1 as a key factor regulating the production and differentiation of YS MΦ progenitors, as well as microglial development. Lyl-1 is one partners of the haematopoietic transcription factor complex which function during developmental haematopoiesis was the least studied. The development of new/more appropriate mouse models should be considered in order to carefully delineate its diverse functions in other resident MΦ populations and possibly other haematopoietic and cardiovascular lineages.

MATERIALS AND METHODS

Ethic statement. Mice were housed in the animal facility of Gustave Roussy Institute ("Plate-forme d'évaluation préclinique", licence #H94-076-11). All animal experiments were conducted in compliance with French and European laws and regulations, under authorized project *#2016-030-5798*, approved by officially accredited local institutional animal (committee n°26) and French "Ministère de la Recherche" ethics boards.

Mice and embryos. We used the following mouse strains: 1- C57BL/6 mice from Harlan or Charles Rivers Laboratories, France, referred to as wild type (WT); 2- *Lyl-1*^{LacZ} mice, in which an in-frame insertion of the β-Galactosidase reporter encoding gene *LacZ* replaced the HLH domain and the entire 3' end of the *Lyl-1* gene. Lyl-1 mice were genotyped as described before *(Capron et al., 2006)*. *Lyl-1*$^{LacZ/LacZ}$ males were crossed with WT or *Lyl-1*$^{LacZ/LacZ}$ females to respectively generate *Lyl-1*$^{WT/LacZ}$ or *Lyl-1*$^{LacZ/LacZ}$ embryos. This breeding scheme avoided the possible detection of FDG/Lyl-1 expression in maternally derived MΦ *(Bertrand et al., 2005b)* in early *Lyl-1*$^{WT/LacZ}$ embryos; 3- *Cx3cr1*^{GFP} mice *(Jung et al., 2000)*. *Cx3cr1*$^{GFP/GFP}$ males were crossed with C57BL/6 to generate *Cx3cr1*$^{WT/GFP}$ mice/embryos or to *Lyl-1*$^{LacZ/LacZ}$ females to generate *Cx3cr1*$^{WT/GFP}$*:Lyl-1*$^{WT/LacZ}$ mice/embryos. 4-The *Cx3cr1*$^{GFP/GFP}$*:Lyl-1*$^{LacZ/LacZ}$ double mutant strain was developed from *Cx3cr1*$^{WT/GFP}$*:Lyl-1*$^{WT/LacZ}$ crosses. *Cx3cr1*$^{WT/GFP}$*:Lyl-1*$^{WT/LacZ}$ and *Cx3cr1*$^{WT/GFP}$*:Lyl-1*$^{LacZ/LacZ}$ mice/embryos were obtained by crossing *Cx3cr1*$^{GFP/GFP}$*:Lyl-1*$^{LacZ/LacZ}$ males to C57BL/6 or *Lyl-1*$^{LacZ/LacZ}$ females, respectively. To exclude maternal/placental cell contamination, the *Cx3cr1* transgene was always inherited from the male parent.

The day of vaginal plug observation was considered as E0.5. Pregnant females were sacrificed by cervical dislocation. Pre-somite embryos were staged according to Downs et al. *(Downs and Davies, 1993)*. E8 to E10.5 embryos were staged by somite counting and thereafter according to morphological landmarks.

Tissues preparation and cell counts. YS (E7.5-E10.5) and E10-FL were dissected as described before *(Bertrand et al., 2005a; Kieusseian et al., 2012)*. To perform cytometry analyses of the developing brain, two different protocols were applied:

1- For analyses performed at early stages (E9-E11), the whole brain were dissected and dissociated as previously described *(Alliot et al., 1999)* and further cleaned from surrounding tissues.

2- From E12 to adult stages, microglia were recovered following Percoll (P1644, Sigma) separation, according to *(Mildner et al., 2007)*. After Percoll purification, 100 µl of the cell suspension was used for cell counting and the remaining cells for flow cytometry analyses. To estimate the number of microglia per brain, the percentage of $CD11b^{+}CD45^{lo}F4/80^{+}$ microglia was reported to the cell count recorded for the corresponding sample.

In vitro culture.

Organ culture: YS explants were placed into plates containing "Complete OptiMEM medium", i.e. OptiMEM with Glutamax (51985-042), 1% Penicillin-streptomycin, 0.1% β-mercaptoethanol (all from ThermoFisher) and 10% foetal calf serum (FCS; Hyclone). YS explants were maintained in organ culture at 37°C, 5% CO_2 for 1 day and are referred to as OrgD1-YS.

Clonogenic assay: Whole YS suspension or sorted cells were plated in triplicate at respectively $3x10^3$ or 100-150 cells/mL in Methocult® M3234 (StemCell Technologies Inc.) always supplemented with Stem Cell factor (50ng/mL), EPO (3U/mL), IL-3 (10 ng/mL), all from Peprotech, IL-6 (10 ng/mL, a gift from Sam Burstein, Maryville IL, USA), CSF-1 (10 ng/mL) and TPO (10ng/mL, provided by Kirin Brewery, Tokyo, Japan). Cultures were maintained in a humidified incubator at 37°C, 5% CO_2 and colonies were scored at day 5 for primitive erythrocytes and day 7 for the other progenitor types.

Flow cytometry, FACS-Gal, proliferation and apoptosis assays. See ***Sup. table 5*** for the list of antibodies and dyes used throughout this study. CD31, F4/80, CD45, CD11b and cKit antibodies were used to characterize myeloid cells. Dead cells were excluded by adding 1 μg/mL 7-amino actinomycin or DAPI (Sigma) before acquisition. Acquisitions were performed on a Canto II cytometer and cell sorting using FACS-Aria III or Influx (All from BD Biosciences). Data were analysed using FlowJo (Treestar) software.

FACS-Gal assay: This assay *(Fiering et al., 1991; Guo and Wu, 2008)*, used as a reporter for Lyl-1 expression, allows the flow cytometry characterization of cells that display a β-Gal activity, using its fluorescent substrate (Fluorescein di-β-galactopyranoside (FDG) F1179; Molecular probe; Thermo Fisher).

Apoptosis assays: For apoptosis analysis, microglia were stained with anti-CD45-PECy7, anti-CD11b-APC-eFluor®780 and anti-F4/80-APC, washed and incubated with Annexin V-FITC. 7AAD was added before acquisition.

Proliferation assay (BrdU incorporation): Pregnant WT and *Lyl-1*$^{LacZ/LacZ}$ females were injected with BrdU (10μM) 12 days after plug detection and sacrificed 2 hours later. Microglia were isolated and stained with CD45-PECy7, CD11b-APC-eFluor®780 and F4/80-PE antibodies. Cells were fixed, permeabilised and treated with DNase (1 hour at 37°C) according to kit instruction (BD Pharmingen No. 552598) and BrdU incorporation was revealed using anti-BrdU-APC.

Brain imaging. To assess microglia morphology in E12 embryos, the midbrain was dissected from *Cx3cr1*$^{WT/GFP}$*:Lyl-1*$^{WT/WT}$ and *Cx3cr1*$^{WT/GFP}$*:Lyl-1*$^{LacZ/LacZ}$ embryos and sectioned through the midline. After fixation in 4% paraformaldehyde overnight at 4°C, whole midbrains were washed in phosphate-buffered saline (PBS)/0.1M glycine and incubated overnight in PBS/15% sucrose at 4°C. Midbrains were washed with PBS+0.1% Tween and incubated 90 min. in blocking buffer

(PBS+10% FCS) at room temperature (RT). Midbrains were subsequently immuno-labelled with F4/80-APC overnight at 4°C. After washing, they were incubated 3 min. in PBS+DAPI (1 μg/mL) at RT and washed. Finally, midbrains were placed in the central well of glass-bottom culture dishes (P35G-1.5-10-C; MatTek, USA) filled with PBS+10% FCS. After appropriate orientation of the sample, the well was covered with a 12 mm ∅ glass coverslip. Image stacks were collected using a Leica SP8 confocal microscope. Images were processed using Imaris x 64 (version 7.7.2; Bitplane) and Photoshop 8.0 (Adobe Systems, San Jose, CA) softwares. To unsure an unbiased choice of the cells imaged, taking into account possible changes in cell distribution induced by *Lyl-1* deficiency, we always acquired cells in similar positions regarding the landmark set in the midbrain flat mount, as shown in ***Sup. fig. 4c***.

RT-qPCR analyses. Total RNA was extracted from sorted $CD11b^{+}F4/80^{+}CD45^{low}$ microglia using Trizol (ThermoFisher). After cDNA synthesis using a SuperScript™ VILO™ Master Mix reverse transcriptase (ThermoFisher), quantitative PCR was performed using SYBR Premix Ex TaqII (Tli RNase H Plus, Takara Bio). Reference genes were *Actin*, *Hprt* and *Tubulin*. Gene expressions were normalized to the value obtained from E10-YS MΦ progenitors, E12 WT $Lin^{-}Sca^{+}cKit^{+}$ (LSK) progenitors or E12 WT microglia, and relative gene expression levels were determined by the ΔΔCt method. Gene expression was considered undetectable if Ct values were >35 cycles. The sequences of the primers used are provided in ***Sup. table 6***.

RNA-sequencing.

Sample preparation: MΦ progenitors ($CD45^{+}CD11b^{+}cKit^{+}$) were sorted from E9 ($M\Phi^{Prim}$ progenitor) and E10 ($M\Phi^{Prim}$ + $M\Phi^{T\text{-}Def}$ progenitors) YS pools from either WT or *Lyl-1*$^{LacZ/LacZ}$

embryos. Four biological replicates were prepared for each sample. RNA was extracted as described above.

Sample processing: The RNA integrity (RNA Integrity Score≥7.0) was checked on the Agilent 2100 Bioanalyzer (Agilent) and quantity was determined using Qubit (Invitrogen). SureSelect Automated Strand Specific RNA Library Preparation Kit was used according to manufacturer's instructions with the Bravo Platform. Briefly, 50ng of total RNA sample was used for poly-A mRNA selection using oligo(dT) beads and subjected to thermal mRNA fragmentation. The fragmented mRNA samples were subjected to cDNA synthesis and further converted into double stranded DNA using the reagents supplied in the kit, and the resulting dsDNA was used for library preparation. The final libraries were bar-coded, purified, pooled together in equal concentrations and subjected to paired-end sequencing (2 x 100) on Novaseq-6000 sequencer (Illumina) at Gustave Roussy genomic facility. RNA-seq data have been deposited in the ArrayExpress database at EMBL-EBI (www.ebi.ac.uk/arrayexpress) under accession number E-MTAB-9618.

RNA-sequencing analysis: Quality of RNA-seq reads was assessed with FastQC 0.11.7 and MultiQC 1.5 *(Ewels et al., 2016)*. Low quality reads were trimmed with Trimmomatic 0.33 *(Bolger et al., 2014)*. Salmon 0.9.0 tool *(Patro et al., 2017)* was used for quantifying the expression of transcripts using geneset annotation from Gencode project release M17 for mouse *(Frankish et al., 2019)*. The version of transcriptome reference sequences used was GRCm38.p6.

Statistical analysis was performed using R with the method proposed by Anders and Huber implemented in the DESeq2 Bioconductor package *(Love et al., 2014)*. The differential expression analysis in DESeq2 uses a generalized linear model (GLM) where counts are modelled using a negative binomial distribution. Counts were normalized from the estimated size factors using the median ratio method and a Wald test was used to test the significance of GLM coefficients.

Genes have been considered differentially expressed when adjusted p-value < 0.05 and fold-change > 2.

Data were analysed through the use of Ingenuity® Pathway Analysis (QIAGEN Inc., https://www.qiagenbioinformatics.com/products/ingenuity-pathway-analysis) *(Krämer et al., 2014)*, Gene set enrichment analysis (GSEA; https://www.gsea-msigdb.org/gsea/index.jsp) *(Mootha et al., 2003; Subramanian et al., 2005)*, Morpheus (https://software.broadinstitute.org/morpheus/) and Venny (https://bioinfogp.cnb.csic.es/tools/venny/) softwares.

Statistical analysis. Statistical tests were performed using Prism 7 (GraphPad) Software. Statistical significance is indicated by the exact p-value and/or as *p < 0.05, **p < 0.01, ***p < 0.001 and ****p < 0.0001.

Acknowledgements.

The authors thank Julien Bertrand for critical reading of the manuscript. We are grateful to the staff of the facilities at Gustave Roussy, the animal facility (PFEP, UMS AMMICa UMS 3655/US23, directed by P. Gonin), the imaging facility (PFIC, UMS AMMICa UMS 3655/US23, directed by C. Laplace-Builhe), the genomic facility directed by N. Droin, the bioinformatics facility (G. Meurice), directed by M. Deloger.

This work was supported by fundings from Institut National de la Santé et de la Recherche Médicale to W. Vainchenker, I. Plo and H. Raslova, from Centre National de la Recherche Scientifique and Université de Paris-Saclay to I. Godin, from grants INCA PLBio to I. Plo, "Ligue Nationale contre le Cancer" Certified Team to H. Raslova, “Association pour la Recherche sur le Cancer” (n°4878) to I. Godin, Gustave Roussy (TA DERE 17) to D. Ren, Grant Agency of the Czech Republic (GACR n°19-23154S) to D. Filipp and from fellowships from “Association pour la Recherche sur le Cancer” to A.-L. Kaushik; “Société Française d'Hématologie" to S. Wang and Chinese Scolarship Council fellowships to S. Wang and D. Ren.

Author Information.

The authors declare no competing financial interests.

Correspondence should be addressed to I.G. (Isabelle.Godin@gustaveroussy.fr).

REFERENCES

Alliot, F., Godin, I., and Pessac, B. (1999). Microglia derive from progenitors, originating from the yolk sac, and which proliferate in the brain. Brain Res Dev Brain Res *117*, 145-152.

Antony, J.M., Paquin, A., Nutt, S.L., Kaplan, D.R., and Miller, F.D. (2011). Endogenous microglia regulate development of embryonic cortical precursor cells. J Neurosci Res *89*, 286-298.

Azzoni, E., Frontera, V., McGrath, K.E., Harman, J., Carrelha, J., Nerlov, C., Palis, J., Jacobsen, S.E.W., and de Bruijn, M.F.T.R. (2018). Kit ligand has a critical role in mouse yolk sac and aorta-gonad-mesonephros hematopoiesis. EMBO reports.

Balounova, J., Splichalova, I., Dobesova, M., Kolar, M., Fiser, K., Prochazka, J., Sedlacek, R., Jurisicova, A., Sung, H.K., Korinek, V.*, et al.* (2019). Toll-like receptor 2 expression on c-kit(+) cells tracks the emergence of embryonic definitive hematopoietic progenitors. Nat Commun *10*, 5176.

Bertrand, J.Y., Giroux, S., Cumano, A., and Godin, I. (2005a). Hematopoietic stem cell development during mouse embryogenesis. Methods Mol Med *105*, 273-288.

Bertrand, J.Y., Jalil, A., Klaine, M., Jung, S., Cumano, A., and Godin, I. (2005b). Three pathways to mature macrophages in the early mouse yolk sac. Blood *106*, 3004-3011.

Bisht, K., Sharma, K., and Tremblay, M.-È. (2018). Chronic stress as a risk factor for Alzheimer's disease: Roles of microglia-mediated synaptic remodeling, inflammation, and oxidative stress. Neurobiology of Stress *9*, 9-21.

Bolger, A.M., Lohse, M., and Usadel, B. (2014). Trimmomatic: a flexible trimmer for Illumina sequence data. Bioinformatics *30*, 2114-2120.

Capron, C., Lécluse, Y., Kaushik, A.L., Foudi, A., Lacout, C., Sekkai, D., Godin, I., Albagli, O., Poullion, I., Svinartchouk, F.*, et al.* (2006). The SCL relative LYL-1 is required for fetal and adult hematopoietic stem cell function and B-cell differentiation. Blood *107*, 4678-4686.

Chiu, S.K., Orive, S.L., Moon, M.J., Saw, J., Ellis, S., Kile, B.T., Huang, Y., Chacon, D., Pimanda, J.E., Beck, D.*, et al.* (2019). Shared roles for Scl and Lyl1 in murine platelet production and function. Blood *134*, 826-835.

Colangelo, V., Schurr, J., Ball, M.J., Pelaez, R.P., Bazan, N.G., and Lukiw, W.J. (2002). Gene expression profiling of 12633 genes in Alzheimer hippocampal CA1: transcription and neurotrophic factor down-regulation and up-regulation of apoptotic and pro-inflammatory signaling. J Neurosci Res *70*, 462-473.

Crotti, A., and Ransohoff, R.M. (2016). Microglial Physiology and Pathophysiology: Insights from Genome-wide Transcriptional Profiling. Immunity *44*, 505-515.

Cumano, A., Dieterlen-Lievre, F., and Godin, I. (1996). Lymphoid potential, probed before circulation in mouse, is restricted to caudal intraembryonic splanchnopleura. Cell *86*, 907-916.

Cumano, A., Ferraz, J.C., Klaine, M., Di Santo, J.P., and Godin, I. (2001). Intraembryonic, but not yolk sac hematopoietic precursors, isolated before circulation, provide long-term multilineage reconstitution. Immunity *15*, 477-485.

Cumano, A., and Godin, I. (2007). Ontogeny of the hematopoietic system. Annu Rev Immunol *25*, 745-785.

Curtis, D.J., Salmon, J.M., and Pimanda, J.E. (2012). Concise Review: Blood Relatives: Formation and regulation of hematopoietic stem cells by the basic helix-loop-helix transcription factors stem cell leukemia and lymphoblastic leukemia-derived sequence 1. Stem Cells *30*, 1053-1058.

Downs, K.M., and Davies, T. (1993). Staging of gastrulating mouse embryos by morphological landmarks in the dissecting microscope. Development *118*, 1255-1266.

Epelman, S., Lavine, K.J., Beaudin, A.E., Sojka, D.K., Carrero, J.A., Calderon, B., Brija, T., Gautier, E.L., Ivanov, S., Satpathy, A.T.*, et al.* (2014). Embryonic and Adult-Derived Resident Cardiac Macrophages Are Maintained through Distinct Mechanisms at Steady State and during Inflammation. Immunity *40*, 91-104.

Ewels, P., Magnusson, M., Lundin, S., and Käller, M. (2016). MultiQC: summarize analysis results for multiple tools and samples in a single report. Bioinformatics *32*, 3047-3048.

Ferrero, G., Mahony, C.B., Dupuis, E.o., Yvernogeau, L., Di Ruggiero, E., Miserocchi, M., Caron, M., Robin, C., Traver, D., Bertrand, J.Y.*, et al.* (2018). Embryonic Microglia Derive from Primitive Macrophages and Are Replaced by cmyb-Dependent Definitive Microglia in Zebrafish. Cell Reports *24*, 130-141.

Ferrier, R., Nougarede, R., Doucet, S., Kahn-Perles, B., Imbert, J., and Mathieu-Mahul, D. (1999). Physical interaction of the bHLH LYL1 protein and NF-kappaB1 p105. Oncogene *18*, 995-1005.

Fiering, S.N., Roederer, M., Nolan, G.P., Micklem, D.R., Parks, D.R., and Herzenberg, L.A. (1991). Improved FACS-Gal: flow cytometric analysis and sorting of viable eukaryotic cells expressing reporter gene constructs. Cytometry *12*, 291-301.

Frankish, A., Diekhans, M., Ferreira, A.M., Johnson, R., Jungreis, I., Loveland, J., Mudge, J.M., Sisu, C., Wright, J., Armstrong, J.*, et al.* (2019). GENCODE reference annotation for the human and mouse genomes. Nucleic Acids Res *47*, D766-d773.

Friedman, B.A., Srinivasan, K., Ayalon, G., Meilandt, W.J., Lin, H., Huntley, M.A., Cao, Y., Lee, S.-H., Haddick, P.C.G., Ngu, H.*, et al.* (2018). Diverse Brain Myeloid Expression Profiles Reveal Distinct Microglial Activation States and Aspects of Alzheimer's Disease Not Evident in Mouse Models. Cell Reports *22*, 832-847.

Ginhoux, F., Greter, M., Leboeuf, M., Nandi, S., See, P., Gokhan, S., Mehler, M.F., Conway, S.J., Ng, L.G., Stanley, E.R.*, et al.* (2010). Fate Mapping Analysis Reveals That Adult Microglia Derive from Primitive Macrophages. Science *330*, 841-845.

Ginhoux, F., and Guilliams, M. (2016). Tissue-Resident Macrophage Ontogeny and Homeostasis. Immunity *44*, 439-449.

Giroux, S., Kaushik, A.L., Capron, C., Jalil, A., Kelaidi, C., Sablitzky, F., Dumenil, D., Albagli, O., and Godin, I. (2007). lyl-1 and tal-1/scl, two genes encoding closely related bHLH transcription factors, display highly overlapping expression patterns during cardiovascular and hematopoietic ontogeny. Gene Expr Patterns *7*, 215-226.

Goldmann, T., Wieghofer, P., Jordão, M.J.C., Prutek, F., Hagemeyer, N., Frenzel, K., Amann, L., Staszewski, O., Kierdorf, K., Krueger, M.*, et al.* (2016). Origin, fate and dynamics of macrophages at central nervous system interfaces. Nature Immunology *17*, 797-805.

Gomez Perdiguero, E., Klapproth, K., Schulz, C., Busch, K., Azzoni, E., Crozet, L., Garner, H., Trouillet, C., de Bruijn, M.F., Geissmann, F.*, et al.* (2015). Tissue-resident macrophages originate from yolk-sac-derived erythro-myeloid progenitors. Nature *518*, 547-551.

Guo, W., and Wu, H. (2008). Detection of LacZ expression by FACS-Gal analysis. Nature Protocol Exchange

Hagemeyer, N., Kierdorf, K., Frenzel, K., Xue, J., Ringelhan, M., Abdullah, Z., Godin, I., Wieghofer, P., Costa Jordao, M.J., Ulas, T.*, et al.* (2016). Transcriptome-based profiling of yolk sac-derived macrophages reveals a role for Irf8 in macrophage maturation. EMBO J *35*, 1730-1744.

Herbomel, P., Thisse, B., and Thisse, C. (2001). Zebrafish early macrophages colonize cephalic mesenchyme and developing brain, retina, and epidermis through a M-CSF receptor-dependent invasive process. Dev Biol *238*, 274-288.

Hoeffel, G., Chen, J., Lavin, Y., Low, D., Almeida, F.F., See, P., Beaudin, A.E., Lum, J., Low, I., Forsberg, E.C.*, et al.* (2015). C-Myb+ Erythro-Myeloid Progenitor-Derived Fetal Monocytes Give Rise to Adult Tissue-Resident Macrophages. Immunity *42*, 665-678.

Hoeffel, G., and Ginhoux, F. (2018). Fetal monocytes and the origins of tissue-resident macrophages. Cell Immunol *330*, 5-15.

Jung, S., Aliberti, J., Graemmel, P., Sunshine, M.J., Kreutzberg, G.W., Sher, A., and Littman, D.R. (2000). Analysis of fractalkine receptor CX(3)CR1 function by targeted deletion and green fluorescent protein reporter gene insertion. Mol Cell Biol *20*, 4106-4114.

Kierdorf, K., Erny, D., Goldmann, T., Sander, V., Schulz, C., Perdiguero, E.G., Wieghofer, P., Heinrich, A., Riemke, P., Holscher, C.*, et al.* (2013). Microglia emerge from erythromyeloid precursors via Pu.1- and Irf8-dependent pathways. Nat Neurosci *16*, 273-280.

Kieusseian, A., Brunet de la Grange, P., Burlen-Defranoux, O., Godin, I., and Cumano, A. (2012). Immature hematopoietic stem cells undergo maturation in the fetal liver. Development *139*, 3521-3530.

Krämer, A., Green, J., Pollard, J., Jr., and Tugendreich, S. (2014). Causal analysis approaches in Ingenuity Pathway Analysis. Bioinformatics *30*, 523-530.

Lavin, Y., Winter, D., Blecher-Gonen, R., David, E., Keren-Shaul, H., Merad, M., Jung, S., and Amit, I. (2014). Tissue-Resident Macrophage Enhancer Landscapes Are Shaped by the Local Microenvironment. Cell *159*, 1312-1326.

Leid, J., Carrelha, J., Boukarabila, H., Epelman, S., Jacobsen, S.E.W., and Lavine, K.J. (2016). Primitive Embryonic Macrophages are Required for Coronary Development and Maturation. Circulation Research *118*, 1498.

Love, M.I., Huber, W., and Anders, S. (2014). Moderated estimation of fold change and dispersion for RNA-seq data with DESeq2. Genome Biol *15*, 550.

Mass, E. (2018). Delineating the origins, developmental programs and homeostatic functions of tissue-resident macrophages. Int Immunol *30*, 493-501.

Mass, E., Ballesteros, I., Farlik, M., Halbritter, F., Gunther, P., Crozet, L., Jacome-Galarza, C.E., Handler, K., Klughammer, J., Kobayashi, Y.*, et al.* (2016). Specification of tissue-resident macrophages during organogenesis. Science *353*.

Matcovitch-Natan, O., Winter, D.R., Giladi, A., Vargas Aguilar, S., Spinrad, A., Sarrazin, S., Ben-Yehuda, H., David, E., Zelada González, F., Perrin, P.*, et al.* (2016). Microglia development follows a stepwise program to regulate brain homeostasis. Science *353*, aad8670.

McCormack, M.P., Shields, B.J., Jackson, J.T., Nasa, C., Shi, W., Slater, N.J., Tremblay, C.S., Rabbitts, T.H., and Curtis, D.J. (2013). Requirement for Lyl1 in a model of Lmo2-driven early T-cell precursor ALL. Blood *122*, 2093-2103.

McGrath, K.E., Frame, J.M., and Palis, J. (2015). Early hematopoiesis and macrophage development. Seminars in Immunology *27*, 379-387.

Mildner, A., Schmidt, H., Nitsche, M., Merkler, D., Hanisch, U.K., Mack, M., Heikenwalder, M., Bruck, W., Priller, J., and Prinz, M. (2007). Microglia in the adult brain arise from Ly-6ChiCCR2+ monocytes only under defined host conditions. Nat Neurosci *10*, 1544-1553.

Mootha, V.K., Lindgren, C.M., Eriksson, K.F., Subramanian, A., Sihag, S., Lehar, J., Puigserver, P., Carlsson, E., Ridderstråle, M., Laurila, E.*, et al.* (2003). PGC-1alpha-responsive genes involved in oxidative phosphorylation are coordinately downregulated in human diabetes. Nat Genet *34*, 267-273.

Nimmakayalu, M., Horton, V.K., Darbro, B., Patil, S.R., Alsayouf, H., Keppler-Noreuil, K., and Shchelochkov, O.A. (2013). Apparent germline mosaicism for a novel 19p13.13 deletion disrupting NFIX and CACNA1A. Am J Med Genet A *161A*, 1105-1109.

Palis, J. (2016). Hematopoietic stem cell-independent hematopoiesis: emergence of erythroid, megakaryocyte, and myeloid potential in the mammalian embryo. FEBS Lett *590*, 3965-3974.

Palis, J., Robertson, S., Kennedy, M., Wall, C., and Keller, G. (1999). Development of erythroid and myeloid progenitors in the yolk sac and embryo proper of the mouse. Development *126*, 5073-5084.

Palpant, N.J., Wang, Y., Hadland, B., Zaunbrecher, R.J., Redd, M., Jones, D., Pabon, L., Jain, R., Epstein, J., Ruzzo, W.L.*, et al.* (2017). Chromatin and Transcriptional Analysis of Mesoderm Progenitor Cells Identifies HOPX as a Regulator of Primitive Hematopoiesis. Cell Reports *20*, 1597-1608.

Patro, R., Duggal, G., Love, M.I., Irizarry, R.A., and Kingsford, C. (2017). Salmon provides fast and bias-aware quantification of transcript expression. Nat Methods *14*, 417-419.

Pina, C., and Enver, T. (2007). Differential contributions of haematopoietic stem cells to foetal and adult haematopoiesis: insights from functional analysis of transcriptional regulators. Oncogene *26*, 6750-6765.

Pirot, N., Deleuze, V., El-Hajj, R., Dohet, C., Sablitzky, F., Couttet, P., Mathieu, D., and Pinet, V. (2010). LYL1 activity is required for the maturation of newly formed blood vessels in adulthood. Blood *115*, 5270-5279.

Porcher, C., Chagraoui, H., and Kristiansen, M.S. (2017). SCL/TAL1: a multifaceted regulator from blood development to disease. Blood *129*, 2051-2060.

Schulz, C., Gomez Perdiguero, E., Chorro, L., Szabo-Rogers, H., Cagnard, N., Kierdorf, K., Prinz, M., Wu, B., Jacobsen, S.E., Pollard, J.W.*, et al.* (2012). A lineage of myeloid cells independent of Myb and hematopoietic stem cells. Science *336*, 86-90.

Senserrich, J., Batsivari, A., Rybtsov, S., Gordon-Keylock, S., Souilhol, C.l., Buchholz, F., Hills, D., Zhao, S., and Medvinsky, A. (2018). Analysis of Runx1 Using Induced Gene Ablation Reveals Its Essential Role in Pre-liver HSC Development and Limitations of an In Vivo Approach, Vol 11.

Soucie, E.L., Weng, Z., Geirsd√≥ttir, L., Molawi, K., Maurizio, J., Fenouil, R., Mossadegh-Keller, N., Gimenez, G., VanHille, L., Beniazza, M.*, et al.* (2016). Lineage-specific enhancers activate self-renewal genes in macrophages and embryonic stem cells. Science *351*.

Subramanian, A., Tamayo, P., Mootha, V.K., Mukherjee, S., Ebert, B.L., Gillette, M.A., Paulovich, A., Pomeroy, S.L., Golub, T.R., Lander, E.S.*, et al.* (2005). Gene set enrichment analysis: a knowledge-based approach for interpreting genome-wide expression profiles. Proc Natl Acad Sci U S A *102*, 15545-15550.

Thomas, D.M., Francescutti-Verbeem, D.M., and Kuhn, D.M. (2006). Gene expression profile of activated microglia under conditions associated with dopamine neuronal damage. Faseb J *20*, 515-517.

Ueno, M., Fujita, Y., Tanaka, T., Nakamura, Y., Kikuta, J., Ishii, M., and Yamashita, T. (2013). Layer V cortical neurons require microglial support for survival during postnatal development. Nat Neurosci *16*, 543-551.

Utz, S.G., See, P., Mildenberger, W., Thion, M.S., Silvin, A., Lutz, M., Ingelfinger, F., Rayan, N.A., Lelios, I., Buttgereit, A.*, et al.* (2020). Early Fate Defines Microglia and Non-parenchymal Brain Macrophage Development. Cell *181*, 557-573 e518.

Wehrspaun, C.C., Haerty, W., and Ponting, C.P. (2015). Microglia recapitulate a hematopoietic master regulator network in the aging human frontal cortex. Neurobiol Aging *36*, 2443 e2449-2443 e2420.

Wilson, N.K., Foster, S.D., Wang, X., Knezevic, K., Sch¸tte, J., Kaimakis, P., Chilarska, P.M., Kinston, S., Ouwehand, W.H., Dzierzak, E.*, et al.* (2010). Combinatorial Transcriptional Control In Blood Stem/Progenitor Cells: Genome-wide Analysis of Ten Major Transcriptional Regulators. Cell Stem Cell *7*, 532-544.

Wittamer, V., and Bertrand, J.Y. (2020). Yolk sac hematopoiesis: does it contribute to the adult hematopoietic system? Cell Mol Life Sci.

FIGURE LEGENDS

Figure 1: Lyl-1 expression discriminates MΦ^{Prim} from MΦ$^{T\text{-}Def}$ progenitors in the early YS

a. Lyl-1 deficiency leads to an increased production of MΦ progenitors in the early YS: Left: Clonogenic potential of E8 OrgD1-YS cells: The production of MΦ progenitors (CFU-M) was increased in *Lyl-1*$^{LacZ/LacZ}$ OrgD1-YS (n=3-5, each sample containing 3-6 YS; mean ± s.e.m.; Unpaired, two-tailed *t*-Test). The size of the MΦ colonies and the cell morphology were similar for the 3 genotypes (data not shown). Right: The distribution of other progenitors with a myeloid potential (EMP and GM) was similar in WT, *Lyl-1*$^{WT/LacZ}$ and *Lyl-1*$^{LacZ/LacZ}$ E8 OrgD1-YS.

b. While all MΦ progenitors in E9-YS (left panel) expressed FDG/Lyl-1, E9.5 and E10-YS (middle panels) harboured two MΦ progenitors subsets discriminated by their FDG/Lyl-1 expression. FDG$^+$/Lyl-1$^+$ and FDG$^-$/Lyl-1$^-$ mature MΦ (CD11b$^+$F4/80$^+$) also coexisted in E10-YS (right). Lyl-1 expression in MΦ progenitors was analysed by FACS-Gal assay, using the β-Gal fluorescent substrate FDG as a reporter for Lyl-1 expression. The contour plots in WT samples indicate the level of non-specific background β-Gal activity/FDG labelling in WT samples. Representative profiles of 3 independent samples, each consisting of 3-4 YS *(See the gating strategy in Sup. fig. 1a)*.

c. MΦ^{Prim} progenitors express Lyl-1. Upper panel: Flow cytometry profiles of WT (left) and *Lyl-1*$^{WT/LacZ}$ (middle left) E8-YS (0-3S). CD11b$^+$CD31$^-$ MΦs (top gate) correspond to maternal MΦ present at this early stage *(Bertrand et al., 2005)*. All CD11b$^+$CD31$^+$ MΦ progenitors (lower gate) displayed FDG/Lyl-1 expression.

d. FDG/Lyl-1 positive and negative myeloid progenitors produce a distinct progeny: The type of progenitors produced by sorted Ter119-cKit$^+$CD45$^+$CD11b$^+$ myeloid progenitors was determined by clonogenic assays using E9 WT and *Lyl-1*$^{WT/LacZ}$ YS (<18 S; n=7), and E10 WT YS (n=15) in 3 independent experiments. At E10, myeloid progenitors from *Lyl-1*$^{WT/LacZ}$ YS were subdivided into FDG/Lyl-1 negative (n=15) and positive (n=12) fractions (5 independent experiments). Samples were biological replicates comprising 6-8 YS. 100 to 150 cKit$^+$CD45$^+$CD11b$^+$ cells per condition were platted in triplicate. FDG$^+$/Lyl-1$^+$ progenitors essentially produced MΦ colonies, while FDG$^-$/Lyl-1$^-$ progenitors produced also GM and G colonies, thus belonging to the transient definitive wave.

e. RT-qPCR quantification of *cMyb* expression levels in cKit$^+$CD45$^+$CD11b$^+$ MΦ progenitors sorted from WT E9-YS, WT and *Lyl-1*$^{WT/LacZ}$ E10-YS, as well as from the FDG/Lyl-1 positive and negative fractions of MΦ progenitors from *Lyl-1*$^{WT/LacZ}$ E10-YS. Lin$^-$Sca$^+$cKit$^+$ (LSK) progenitors from WT E12 FL were used as positive control. FDG$^+$/Lyl-1$^+$ MΦ progenitors from E10-YS expressed *cMyb*$^{Low/Neg}$ levels similar to E9-YS, which characterize the primitive YS wave. The FDG$^-$/Lyl-1$^-$ fraction expressed significantly higher *cMyb* levels, similar to LSK cells from E12-FL. *cMyb* expression levels, shown on a Log^2 scale, were normalized to the mean expression value obtained for WT E10-YS, considered as 1 (Unpaired, two-tailed *t*-Test).

f. Differentially expressed genes in MΦ progenitors ($CD45^+CD11b^+cKit^+$) sorted from WT and *Lyl-1*$^{LacZ/LacZ}$ YS at E9 and E10. Upper panel: Unsupervised principal component analysis (PCA) plot positioned E9 and E10 MΦ progenitors in two distinct groups, followed by segregation of WT and *Lyl-1*$^{LacZ/LacZ}$ samples. Lower panel: Volcano plot of E9 WT vs E10 WT MΦ progenitors. Red and green dots indicate genes with statistically significant changes in expression level. (*p*-value <0.05, absolute fold change≥2.0) (NDE: not deregulated genes; DE-Up: up-regulated genes; DE-Down: down-regulated genes).

g. Upper panel: Venn diagram comparing DEGs in E9 WT versus E10 WT MΦ progenitors to the EMP (Left) or MΦ signatures defined by *(Mass et al., 2016)* (GEO accession number GSE81774). The number and percentage of DEGs common to the EMP or MΦ signatures is shown.

Lower panel: Expression profiles of the overlapping genes identified by the Venn diagram (Heatmap displays transformed log2-expression values; Unpaired *t*-Test, two-tailed). Note the higher expression at E10 of genes involved in erythroid (Haemoglobins: Pink arrow; Transcription factors: green arrow), as well as megakaryocytic and granulocytic-related genes (blue arrow).

h. Relative expression levels of *Gata1* and *Spi1/*PU.1, as indicated by their relative Transcripts per million kilo-bases (TPM).

i. Enriched Pathways in E9 and E10 WT MF progenitors with absolute z-score ≥2, from QIAGEN's Ingenuity® Pathway Analysis (IPA). Bars: minus log of the p-value of each canonical pathway; Orange line: threshold p-value of 0.05. Ratio: genes detected/genes per pathway.

j. Expression profiles of DEGs related to IFNγ and IFNβ response, identified by g:Profiler. (Heatmap displays transformed log2-expression values; unpaired t-Test, two-tailed).

k. Expression profiles of DEGs related to MHC-II complex (Heatmap displays transformed log2-expression values; unpaired *t*-Test, two-tailed).

l. Expression profiles of DEGs related to cytokine signalling (Heatmap displays transformed log2-expression values; unpaired *t*-Test, two-tailed).

Figure 2:

a. Lyl-1 regulates the production of E8 MΦ^{Prim} progenitors.

Left panel: Flow cytometry quantification of FDG^+/Lyl-$1^+CD11b^+CD31^+$ MΦ progenitors from WT and *Lyl-1*$^{WT/LacZ}$ E8-YS (0-3S). The MΦ progenitor subset was enlarged in *Lyl-1*$^{WT/LacZ}$ YS (right; n=3).

Right panel: In clonogenic assays, less than one EMP and/or GM progenitor per E8-YS was detected in WT and mutant samples, confirming that the assay was performed at a time when EMP-derived-MΦ progenitors were absent. The majority of the 25-30 colonies per YS were Ery^P (60 to 80% in the 3 genotypes). The number of MΦ colonies obtained from E8-YS (0-3S) was increased in *Lyl-1*$^{WT/LacZ}$ and *Lyl-1*$^{LacZ/LacZ}$ compared to WT (left). Other progenitors were occasionally and randomly found in the *Lyl-1*$^{WT/LacZ}$

FDG$^+$/Lyl-1$^+$ fraction including EMPs (0.81%±0.66; n=3). (n=3-5, each sample contained 5-10 YS; plots show mean ± s.e.m.; Unpaired, two-tailed *t*-Test).

b. The relative expression levels (read counts) of the CD41 coding gene *Itg2b* is increased in *Lyl-1*$^{lacZ/lacZ}$ MΦ progenitors compared to WT at E9 (unpaired *t*-Test, two-tailed).

c. Relative expression levels of transcriptions factors regulating haematopoietic progenitor emergence in *Lyl-1*$^{LacZ/LacZ}$ MΦ progenitors compared to WT at E9 (*p*-values were determined by unpaired, two-tailed *t*-Test).

d. GSEA pathways (Top; FDR q-Value <0.29) and GO terms (Bottom; FDR q-value <0.01) enriched in E9 *Lyl-1*$^{lacZ/lacZ}$ compared to E9 WT MΦ progenitors. Highlighted are the pathways specifically related to embryo patterning (blue) and to the development of skeletal (green) and nervous systems (yellow). Pink arrows point to changes related to metabolic pathways.

Figure 3: **The differentiation MΦ progenitors is defective in *Lyl-1*$^{LacZ/LacZ}$ YS.**

a. Distribution of A1-A2 and A3 MΦ subsets in E10-YS from *Cx3cr1*$^{WT/GFP}$*:Lyl-1*$^{WT/WT}$, *Cx3cr1*$^{WT/GFP}$*:Lyl-1*$^{WT/LacZ}$ and *Cx3cr1*$^{WT/GFP}$*:Lyl-1*$^{LacZ/LacZ}$ embryos. While the size of the whole MΦ population is similar in the three genotypes (Top panel), *Lyl-1* deficiency leads to a modified distribution of the MΦ subsets (middle and lower panel) with an increased size of the A1 subset and a reduced A3 pool (5-12 independent analyses, each sample cumulating 6-8 YS. Plots show mean ± s.e.m.; Unpaired, two-tailed *t*-Test).

b. GSEA pathway indicates a deficit in Jak1-Stat signalling in *Lyl-1*$^{LacZ/LacZ}$ MΦ progenitors compared to WT at E9 (NES: normalised enrichment score; FDR: false discovery rate).

c. Relative expression levels (read counts) of haematopoietic markers in WT and *Lyl-1*$^{LacZ/LacZ}$ MΦ progenitors at E9 (unpaired *t*-Test, two-tailed).

d. Top 1 GSEA pathway indicates that the IFN signalling pathway (left) which characterize E9 MΦ^{Prim} progenitors, and particularly *Irf8* (right), is defective in *Lyl-1*$^{LacZ/LacZ}$ MΦ progenitors (NES: normalised enrichment score; FDR: false discovery rate).

e. From the 53 canonical pathways identified by IPA in the DEGs, 9 were enriched with an absolute Z score ≥ 1. Bars: minus log of the *p*-value of each canonical pathway; Orange line: threshold p-value of 0.05. Ratio: genes detected/genes per pathway.

f. Upper panel: Venn diagram comparing the DEGs in E9 *Lyl-1*$^{LacZ/LacZ}$ vs E9 WT to those in E10 *Lyl-1*$^{LacZ/LacZ}$ vs E10 WT MΦ progenitors. Lower panel: Expression profiles of the DEGs common to both stages identified by the Venn comparison (Heatmap displays transformed log2-expression values; unpaired *t*-Test, two-tailed).

Figure 4:

a. Left panel: All MΦ progenitors from E10-Brain (Left) expressed Lyl-1, contrary to the corresponding YS (Fig. 1b right) which harbour both FDG^+/Lyl-1^+ and FDG^-/Lyl-1^- subsets. MΦ progenitors from E10 *Lyl-1*$^{LacZ/LacZ}$ FL (right) harboured both FDG^+/Lyl-1^+ and FDG^-/Lyl-1 MΦ progenitors subsets. Right panel: in E10 brain, mature MΦ ($CD11b^+F4/80^+$ gate) were all FDG^+/Lyl-1^+

The contour plots in WT samples indicate the level of non-specific background β-Gal activity/FDG labelling in WT samples. Representative profiles of 3 independent samples, each consisting of 3-4 Brain or 8-12 E10-FL.

b. Quantification of $cKit^+CD45^+CD11b^+$ MΦ progenitors in E10-FL (plots show mean ± s.e.m.; Unpaired, two-tailed *t*-Test).

c. Lyl-1 marks the entire F4/80+ microglia/BAM population from the onset of brain colonisation. The rare CD11b+ F4/80$^{low\text{-}neg}$ cells present in the brain at E9 are FDG/Lyl-positive (Top Panel)**.** Grey histograms indicate non-specific background β-Gal activity/FDG levels in WT samples.

d. MΦ progenitors from E10 brain expressed *cMyb* levels similar to E9-YS MΦ^{Prim} progenitors. RT-qPCR quantification of *cMyb* expression levels in $cKit^+CD45^+CD11b^+$ MΦ progenitors sorted from WT E9-YS and from WT and *Lyl-1*$^{WT/LacZ}$ brain at E10. $Lin^-Sca^+cKit^+$ (LSK) progenitors from WT E12 FL were used as positive control. *cMyb* expression levels, shown on a Log^2 scale, were normalized to the mean expression value obtained for WT E10-YS, considered as 1 (Unpaired, two-tailed *t*-Test).

e. Heatmap showing the expression profiles of the DEGs in E9 WT vs E10 WT MΦ^{Prim} progenitors that mark the development of tissue resident MΦ (Heatmap displays transformed log2-expression values; Unpaired, two-tailed *t*-Test).

f. RT-qPCR analyses of *Lyl-1* expression in A1 to A3 MΦ subsets isolated from Cx3cr1$^{WT/GFP}$ brain at E10. *Lyl-1* is expressed by the 3 subsets, with levels decreasing with differentiation. Expression levels were normalized to the mean value obtained for Cx3cr1$^{WT/GFP}$ YS A1 progenitors (n=3).

g. Defective differentiation of brain MΦ progenitor in Lyl-1 mutant embryos. Distribution of A1-A2 and A3 MΦ subsets in E10 brain from Cx3cr1$^{WT/GFP}$:Lyl-1$^{WT/WT}$, Cx3cr1$^{WT/GFP}$:Lyl-1$^{WT/LacZ}$ and Cx3cr1$^{WT/GFP}$:Lyl-1$^{LacZ/LacZ}$ embryos. The size of the whole MΦ population was similar in the three genotypes (Top panel), but Lyl-1 deficiency modified the distribution of the MΦ subsets (middle and lower panel) with an increased size of the A1 subset and a reduced A3 pool (5-12 independent analyses, each sample cumulating brains from 6-8 embryos. Plots show mean ± s.e.m.; Unpaired, two-tailed t Test).

Figure 5: Lyl-1 deficiency leads to transient reductions of the microglia pool at E12 and P0-P3.

a. Quantification of the microglia population in E12 and E14 brain showing the decreased size of the microglia pool at E12 and its recovery to a normal pool size at E14. Plots show mean ± s.e.m.; Two tailed, unpaired *t*-test.

b. A reduced microglia proliferation may account for the reduced microglia number at E12, as shown by the two folds decrease (right) of BrdU-labelled cells in *Lyl-1*$^{LacZ/LacZ}$ (middle) compared to WT (left) brains. Plots show mean±s.e.m.; Two tailed, unpaired *t*-test.

c. At E12, *Cx3cr1*$^{WT/GFP}$*:Lyl-1*$^{LacZ/LacZ}$ microglia displayed a reduced number and extent of ramifications compared to their *Cx3cr1*$^{WT/GFP}$ counterpart. Bottom: Microglia morphology was classified into subtypes depending on the number of main ramifications (A: none, B: 2, C: 3 and D:>3). Top: Microglia deprived of ramifications predominated in *Lyl-1*-deficient microglia. 65 and 61 cells were respectively acquired from the midbrain of E12 *Cx3cr1*$^{WT/GFP}$ and *Cx3cr1*$^{WT/GFP}$*:Lyl-1*$^{LacZ/LacZ}$ embryos (for each genotype, brains from 12 embryos were acquired in 3 independent experiments). Microglia were identified by *Cx3cr1*-driven GFP expression and F4/80-APC immuno-staining. Bar=10mm. Plots show mean±s.e.m.; Two tailed, unpaired *t*-test.

d. In *Lyl-1*$^{LacZ/LacZ}$ new-borns, the cellularity of the brain was consistently lower than in WT (left), and so was the estimated microglia number (right). Plots show mean ± s.e.m.; Two tailed, unpaired *t*-test.

e. Kinetic evolution of *Lyl-1* expression levels in WT microglia from embryonic stages to adulthood. An increased expression of *Lyl-1* from embryonic stages to adulthood was also inferred from timeline RNA-seq. data *(Matcovitch-Natan et al., 2016)* (GEO accession number GSE79812).

f. Quantitative RT-PCR analyses also point to E12 and P0 as key development stages regulated by Lyl-1. CD11b^{+}F4/80^{+}CD45^{low} microglia were isolated at sequential development stages. Bar graphs show the kinetic of expression of genes modified in *Lyl-1*$^{LacZ/LacZ}$ microglia (arrowheads), normalized to the mean expression value in WT E12 microglia (n=3). Error bars indicate s.e.m. Two tailed, unpaired *t*-test.

g. *Cx3Cr1* and Lyl-1 expression in mutant microglia. The expression level of *Cx3CR1*, analysed as in f, was decreased in Lyl-1 mutant at E12 (left), while *Lyl-1* expression level was unmodified in *CX3CR1*$^{GFP/GFP}$ microglia at E12 and in new-borns (right).

h. *Mafb* expression in mutant microglia. *Mafb* expression level, analysed as in f, was reduced in the microglia of *Lyl-1*$^{LacZ/LacZ}$ new-borns.

i. The expression of genes enriched in microglia and/or essential for their function are deregulated in *Lyl-1*$^{LacZ/LacZ}$ MΦ progenitors at E9. Relative expression levels (read counts) in WT and *Lyl-1*$^{lacZ/lacZ}$ MΦ progenitors from E9 YS (*P* values were determined by unpaired, two-tailed *t*-Test).

References

Bertrand, J.Y., Jalil, A., Klaine, M., Jung, S., Cumano, A., and Godin, I. (2005). Three pathways to mature macrophages in the early mouse yolk sac. Blood *106*, 3004-3011.

Mass, E., Ballesteros, I., Farlik, M., Halbritter, F., Gunther, P., Crozet, L., Jacome-Galarza, C.E., Handler, K., Klughammer, J., Kobayashi, Y.*, et al.* (2016). Specification of tissue-resident macrophages during organogenesis. Science.

Matcovitch-Natan, O., Winter, D.R., Giladi, A., Vargas Aguilar, S., Spinrad, A., Sarrazin, S., Ben-Yehuda, H., David, E., Zelada González, F., Perrin, P.*, et al.* (2016). Microglia development follows a stepwise program to regulate brain homeostasis. Science *353*, aad8670.

Figure 1

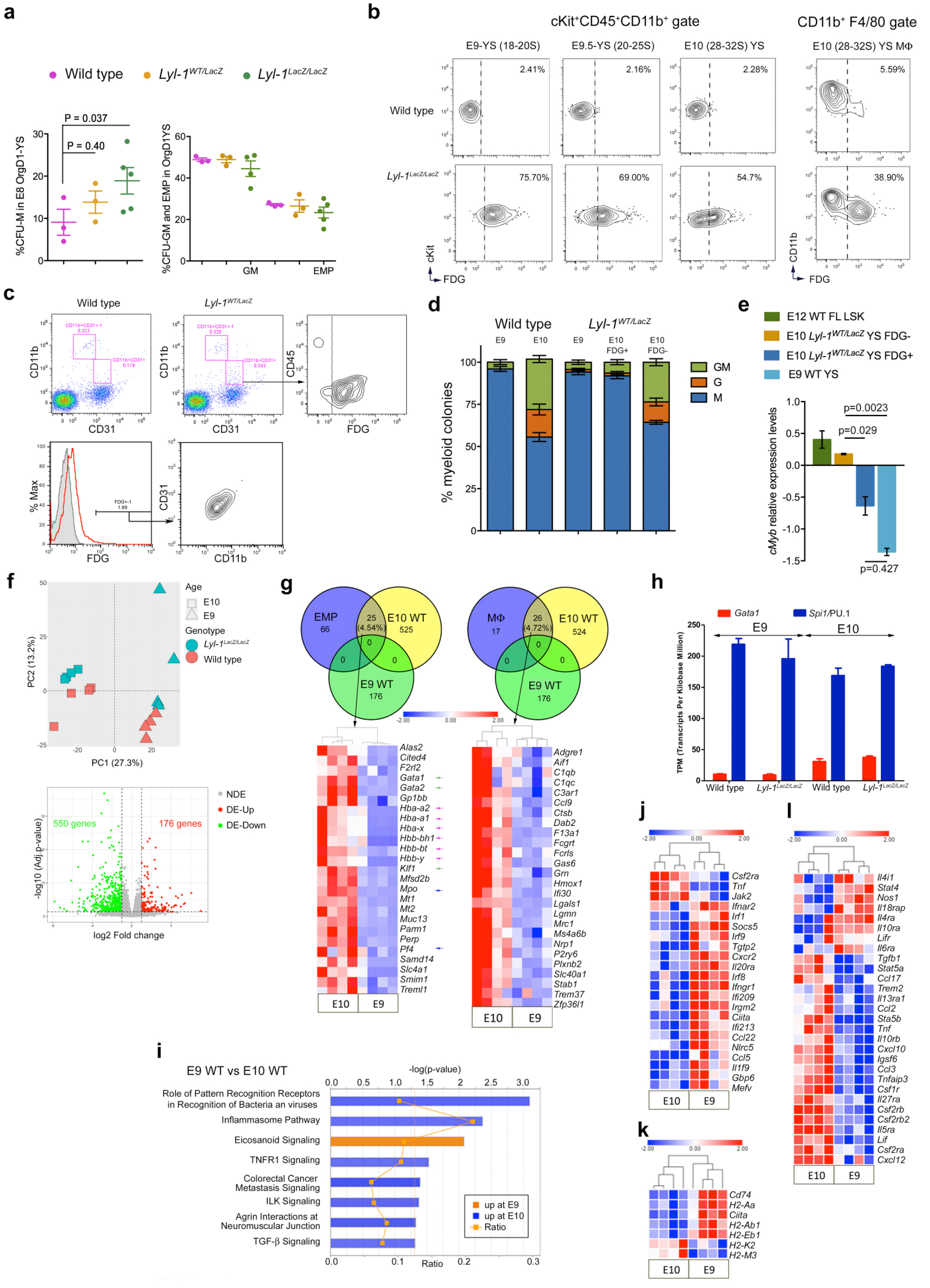
a
Wild type
Lyl-1WT/LacZ
Lyl-1LacZ/LacZ
P = 0.037
P = 0.40
%CFU-M in E8 OrgD1-YS
%CFU-GM and EMP in OrgD1YS
GM
EMP
b
cKit+CD45+CD11b+ gate
CD11b+ F4/80 gate
E9-YS (18-20S)
E9.5-YS (20-25S)
E10 (28-32S) YS
E10 (28-32S) YS MΦ
Wild type
Lyl-1LacZ/LacZ
2.41%
2.16%
2.28%
5.59%
75.70%
69.00%
54.7%
38.90%
cKit
CD11b
FDG
c
Wild type
Lyl-1WT/LacZ
CD11b
CD31
CD45
FDG
% Max
d
Wild type
Lyl-1WT/LacZ
E9
E10
E10 FDG+
E10 FDG-
% myeloid colonies
GM
G
M
e
E12 WT FL LSK
E10 Lyl-1WT/LacZ YS FDG-
E10 Lyl-1WT/LacZ YS FDG+
E9 WT YS
cMyb relative expression levels
p=0.0023
p=0.029
p=0.427
f
Age
E10
E9
Genotype
Lyl-1LacZ/LacZ
Wild type
PC2 (13.2%)
PC1 (27.3%)
NDE
DE-Up
DE-Down
550 genes
176 genes
-log10 (Adj.p-value)
log2 Fold change
g
EMP
66
25
(4.54%)
E10 WT
525
E9 WT
176
MΦ
17
26
(4.72%)
E10 WT
524
E9 WT
176
Alas2
Cited4
F2rl2
Gata1
Gata2
Gp1bb
Hba-a2
Hba-a1
Hba-x
Hbb-bh1
Hbb-bt
Hbb-y
Klf1
Mfsd2b
Mpo
Mt1
Mt2
Muc13
Parm1
Perp
Pf4
Samd14
Slc4a1
Smim1
Treml1
Adgre1
Aif1
C1qb
C1qc
C3ar1
Ccl9
Ctsb
Dab2
F13a1
Fcgrt
Fcrls
Gas6
Grn
Hmox1
Ifi30
Lgals1
Lgmn
Mrc1
Ms4a6b
Nrp1
P2ry6
Plxnb2
Slc40a1
Stab1
Trem37
Zfp36l1
E10
E9
h
Gata1
Spi1/PU.1
E9
E10
TPM (Transcripts Per Kilobase Million)
Wild type
Lyl-1LacZ/LacZ
Wild type
Lyl-1LacZ/LacZ
i
E9 WT vs E10 WT
-log(p-value)
Role of Pattern Recognition Receptors in Recognition of Bacteria an viruses
Inflammasome Pathway
Eicosanoid Signaling
TNFR1 Signaling
Colorectal Cancer Metastasis Signaling
ILK Signaling
Agrin Interactions at Neuromuscular Junction
TGF-β Signaling
up at E9
up at E10
Ratio
j
Csf2ra
Tnf
Jak2
Ifnar2
Irf1
Socs5
Irf9
Tgtp2
Cxcr2
Il20ra
Irf8
Ifngr1
Ifi209
Irgm2
Ciita
Ifi213
Ccl22
Nlrc5
Ccl5
Il1f9
Gbp6
Mefv
E10
E9
k
Cd74
H2-Aa
Ciita
H2-Ab1
H2-Eb1
H2-K2
H2-M3
E10
E9
l
Il4i1
Stat4
Nos1
Il18rap
Il4ra
Il10ra
Lifr
Il6ra
Tgfb1
Stat5a
Ccl17
Trem2
Il13ra1
Ccl2
Sta5b
Tnf
Il10rb
Cxcl10
Igsf6
Ccl3
Tnfaip3
Csf1r
Il27ra
Csf2rb
Csf2rb2
Il5ra
Lif
Csf2ra
Cxcl12
E10
E9

Figure 2

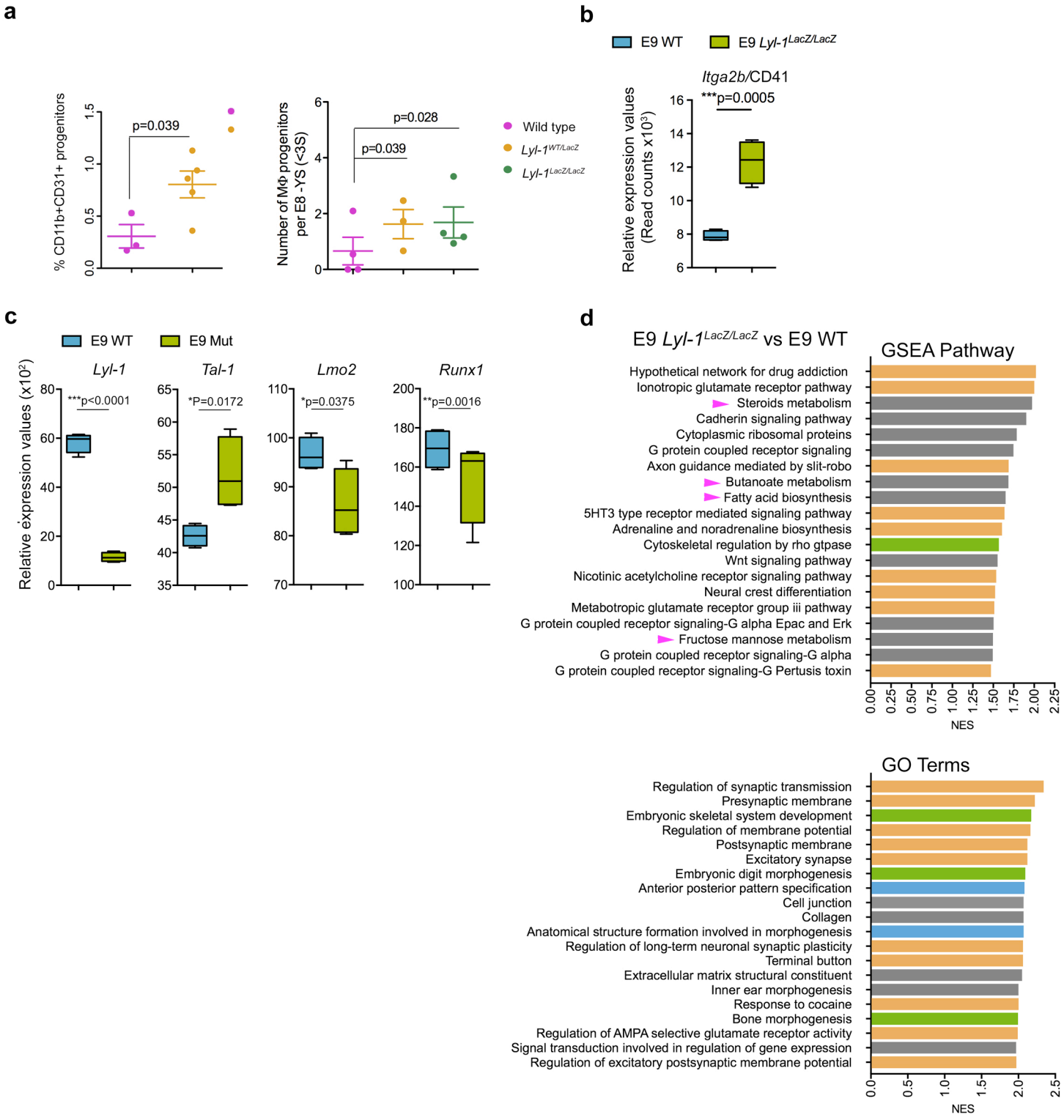
a
% CD11b+CD31+ progenitors
p=0.039
Number of MΦ progenitors per E8 -YS (<3S)
p=0.028
p=0.039
Wild type
Lyl-1WT/LacZ
Lyl-1LacZ/LacZ
b
E9 WT
E9 Lyl-1LacZ/LacZ
Itga2b/CD41
***p=0.0005
Relative expression values (Read counts x10³)
c
E9 WT
E9 Mut
Lyl-1
Tal-1
Lmo2
Runx1
Relative expression values (x10²)
***p<0.0001
*P=0.0172
*p=0.0375
**p=0.0016
d
E9 Lyl-1LacZ/LacZ vs E9 WT
GSEA Pathway
Hypothetical network for drug addiction
Ionotropic glutamate receptor pathway
Steroids metabolism
Cadherin signaling pathway
Cytoplasmic ribosomal proteins
G protein coupled receptor signaling
Axon guidance mediated by slit-robo
Butanoate metabolism
Fatty acid biosynthesis
5HT3 type receptor mediated signaling pathway
Adrenaline and noradrenaline biosynthesis
Cytoskeletal regulation by rho gtpase
Wnt signaling pathway
Nicotinic acetylcholine receptor signaling pathway
Neural crest differentiation
Metabotropic glutamate receptor group iii pathway
G protein coupled receptor signaling-G alpha Epac and Erk
Fructose mannose metabolism
G protein coupled receptor signaling-G alpha
G protein coupled receptor signaling-G Pertusis toxin
NES
GO Terms
Regulation of synaptic transmission
Presynaptic membrane
Embryonic skeletal system development
Regulation of membrane potential
Postsynaptic membrane
Excitatory synapse
Embryonic digit morphogenesis
Anterior posterior pattern specification
Cell junction
Collagen
Anatomical structure formation involved in morphogenesis
Regulation of long-term neuronal synaptic plasticity
Terminal button
Extracellular matrix structural constituent
Inner ear morphogenesis
Response to cocaine
Bone morphogenesis
Regulation of AMPA selective glutamate receptor activity
Signal transduction involved in regulation of gene expression
Regulation of excitatory postsynaptic membrane potential
NES

Figure 3

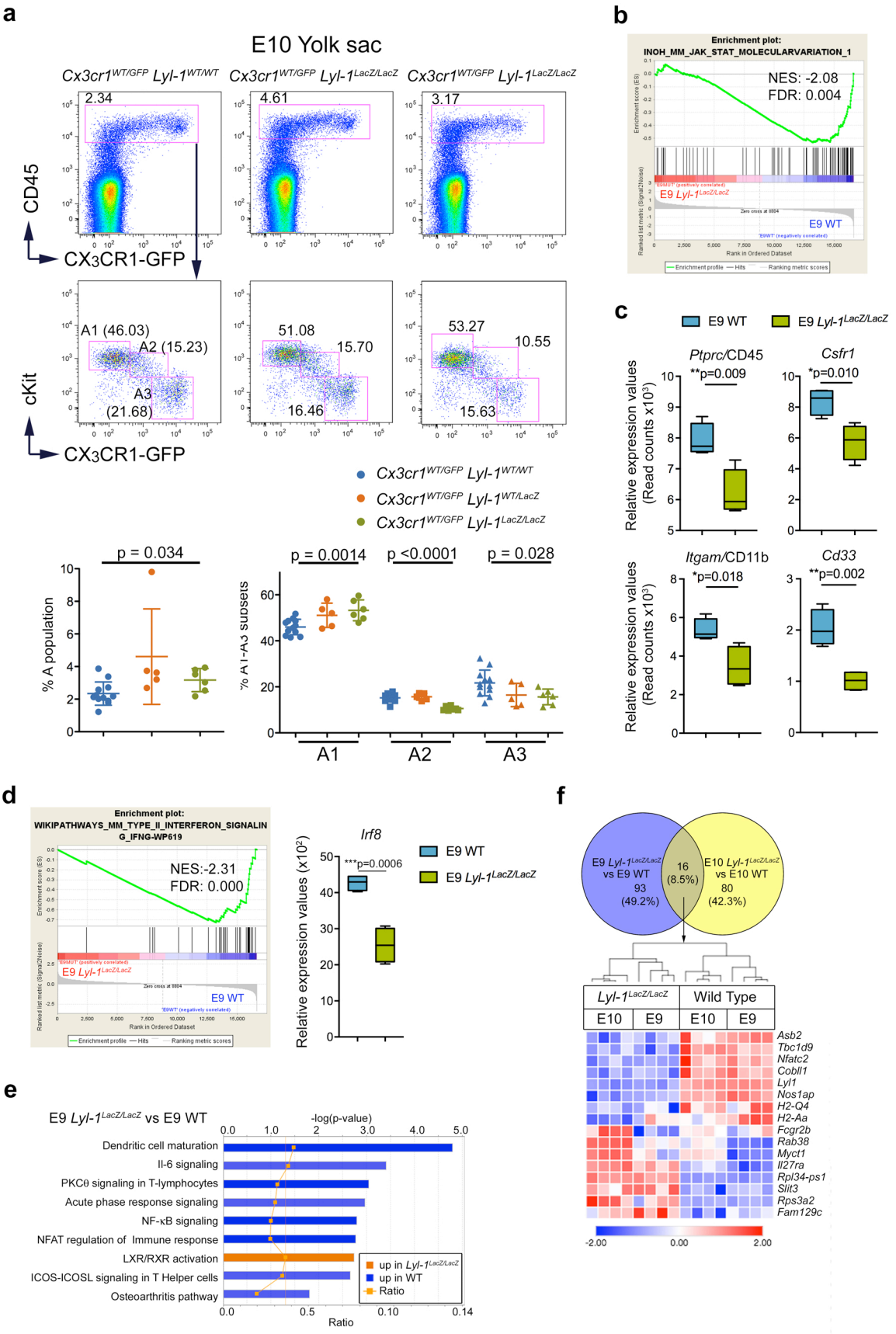
a
E10 Yolk sac
Cx3cr1WT/GFP Lyl-1WT/WT
Cx3cr1WT/GFP Lyl-1LacZ/LacZ
Cx3cr1WT/GFP Lyl-1LacZ/LacZ
2.34
4.61
3.17
CD45
CX3CR1-GFP
A1 (46.03)
A2 (15.23)
A3 (21.68)
51.08
15.70
16.46
53.27
10.55
15.63
cKit
CX3CR1-GFP
Cx3cr1WT/GFP Lyl-1WT/WT
Cx3cr1WT/GFP Lyl-1WT/LacZ
Cx3cr1WT/GFP Lyl-1LacZ/LacZ
p = 0.034
% A population
p = 0.0014
p <0.0001
p = 0.028
% A1-A3 subsets
A1
A2
A3
b
Enrichment plot:
INOH_MM_JAK_STAT_MOLECULARVARIATION_1
NES: -2.08
FDR: 0.004
E9 Lyl-1LacZ/LacZ
E9 WT
Rank in Ordered Dataset
c
E9 WT
E9 Lyl-1LacZ/LacZ
Ptprc/CD45
**p=0.009
Csfr1
*p=0.010
Relative expression values (Read counts x10³)
Itgam/CD11b
*p=0.018
Cd33
**p=0.002
d
Enrichment plot:
WIKIPATHWAYS_MM_TYPE_II_INTERFERON_SIGNALING_IFNG-WP619
NES:-2.31
FDR: 0.000
E9 Lyl-1LacZ/LacZ
E9 WT
Rank in Ordered Dataset
Irf8
***p=0.0006
E9 WT
E9 Lyl-1LacZ/LacZ
Relative expression values (x10²)
e
E9 Lyl-1LacZ/LacZ vs E9 WT
-log(p-value)
Dendritic cell maturation
Il-6 signaling
PKCθ signaling in T-lymphocytes
Acute phase response signaling
NF-κB signaling
NFAT regulation of Immune response
LXR/RXR activation
ICOS-ICOSL signaling in T Helper cells
Osteoarthritis pathway
up in Lyl-1LacZ/LacZ
up in WT
Ratio
Ratio
f
E9 Lyl-1LacZ/LacZ vs E9 WT
93 (49.2%)
16 (8.5%)
E10 Lyl-1LacZ/LacZ vs E10 WT
80 (42.3%)
Lyl-1LacZ/LacZ
Wild Type
E10
E9
E10
E9
Asb2
Tbc1d9
Nfatc2
Cobll1
Lyl1
Nos1ap
H2-Q4
H2-Aa
Fcgr2b
Rab38
Myct1
Il27ra
Rpl34-ps1
Slit3
Rps3a2
Fam129c
-2.00
0.00
2.00

Figure 4

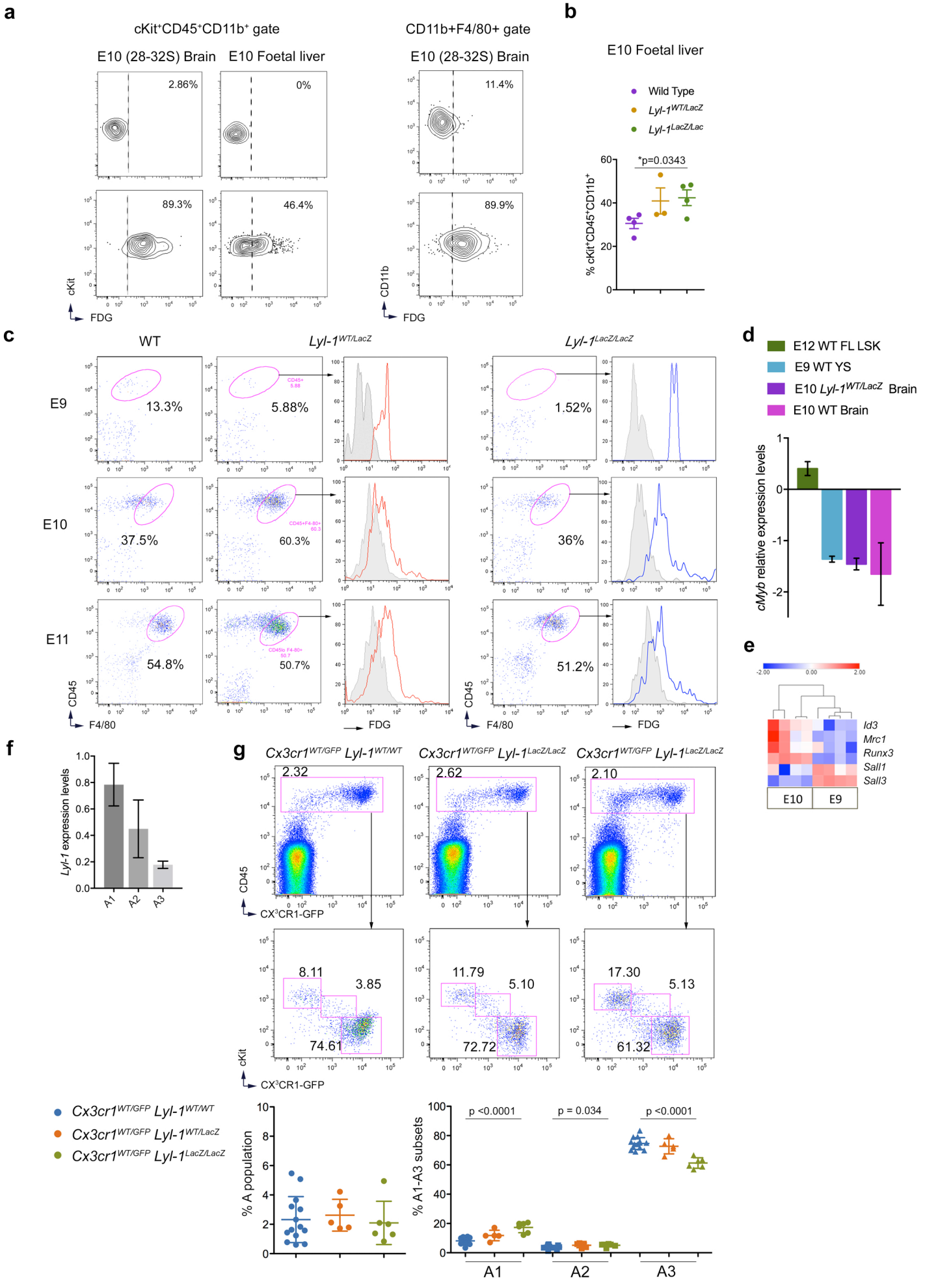
a
cKit+CD45+CD11b+ gate
E10 (28-32S) Brain
E10 Foetal liver
2.86%
0%
89.3%
46.4%
cKit
FDG
CD11b+F4/80+ gate
E10 (28-32S) Brain
11.4%
89.9%
CD11b
FDG
b
E10 Foetal liver
Wild Type
Lyl-1WT/LacZ
Lyl-1LacZ/Lac
*p=0.0343
% cKit+CD45+CD11b+
c
WT
Lyl-1WT/LacZ
Lyl-1LacZ/LacZ
E9
13.3%
5.88%
1.52%
E10
37.5%
60.3%
36%
E11
54.8%
50.7%
51.2%
CD45
F4/80
FDG
d
E12 WT FL LSK
E9 WT YS
E10 Lyl-1WT/LacZ Brain
E10 WT Brain
cMyb relative expression levels
e
Id3
Mrc1
Runx3
Sall1
Sall3
E10
E9
f
Lyl-1 expression levels
A1
A2
A3
g
Cx3cr1WT/GFP Lyl-1WT/WT
Cx3cr1WT/GFP Lyl-1LacZ/LacZ
Cx3cr1WT/GFP Lyl-1LacZ/LacZ
2.32
2.62
2.10
CD45
CX3CR1-GFP
8.11
3.85
74.61
11.79
5.10
72.72
17.30
5.13
61.32
cKit
CX3CR1-GFP
Cx3cr1WT/GFP Lyl-1WT/WT
Cx3cr1WT/GFP Lyl-1WT/LacZ
Cx3cr1WT/GFP Lyl-1LacZ/LacZ
% A population
% A1-A3 subsets
p <0.0001
p = 0.034
p <0.0001
A1
A2
A3

Figure 5

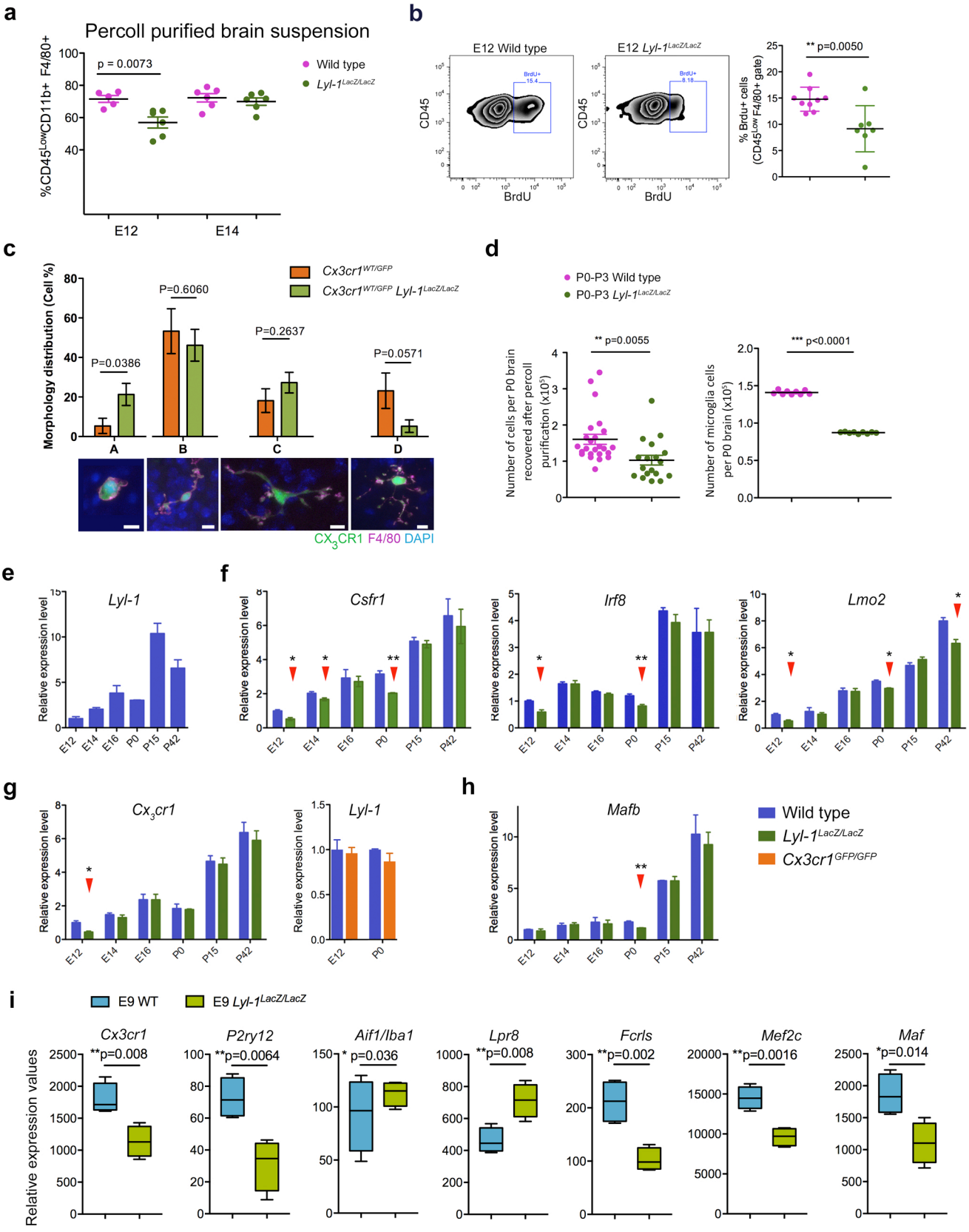
a
Percoll purified brain suspension
%CD45LowCD11b+ F4/80+
p = 0.0073
Wild type
Lyl-1LacZ/LacZ
E12
E14
b
E12 Wild type
E12 Lyl-1LacZ/LacZ
CD45
BrdU
BrdU+ 15.4
BrdU+ 8.18
% Brdu+ cells (CD45Low F4/80+ gate)
** p=0.0050
c
Morphology distribution (Cell %)
Cx3cr1WT/GFP
Cx3cr1WT/GFP Lyl-1LacZ/LacZ
P=0.0386
P=0.6060
P=0.2637
P=0.0571
A
B
C
D
CX3CR1 F4/80 DAPI
d
P0-P3 Wild type
P0-P3 Lyl-1LacZ/LacZ
Number of cells per P0 brain recovered after percoll purification (x10⁵)
** p=0.0055
Number of microglia cells per P0 brain (x10⁵)
*** p<0.0001
e
Lyl-1
Relative expression level
E12
E14
E16
P0
P15
P42
f
Csfr1
Irf8
Lmo2
g
Cx3cr1
Lyl-1
h
Mafb
Wild type
Lyl-1LacZ/LacZ
Cx3cr1GFP/GFP
i
E9 WT
E9 Lyl-1LacZ/LacZ
Relative expression values
Cx3cr1
**p=0.008
P2ry12
**p=0.0064
Aif1/Iba1
* p=0.036
Lpr8
**p=0.008
Fcrls
**p=0.002
Mef2c
**p=0.0016
Maf
*p=0.014